Western University
Scholarship@Western

Earth Sciences Publications

Earth Sciences Department

2019

Fluid-present Anatexis of Neoarchean Tonalite and Amphibolite in the Western Shandong Province

Chris Yakymchuk
University of Waterloo

Wenran Zhao
University of Waterloo

Yusheng Wan
Chinese Academy of Geological Sciences

Shoufa Lin
University of Waterloo

Fred Longstaffe
The University of Western Ontario, flongsta@uwo.ca

Fluid-present anatexis of Neoarchean tonalite and amphibolite in the Western Shandong Province

Chris Yakymchuk[1*], Wenran Zhao[1], Yusheng Wan[2], Shoufa Lin[1], Fred J. Longstaffe[3]

[1]*Department of Earth and Environmental Sciences, University of Waterloo, 200 University Ave West, Waterloo, Ontario, Canada (*cyakymchuk@uwaterloo.ca)*

[2] *Beijing SHRIMP Center, Institute of Geology, Chinese Academy of Geological Sciences, 26 Baiwanzhuang Road, Beijing 100037, China*

[3]*Department of Earth Sciences, The University of Western Ontario, London, Ontario N6A5B7, Canada*

Highlights
- Fluid-present anatexis at ~2.60 Ga reworked metatonalites and amphibolites
- Melt compositions were modified by plagioclase and hornblende accumulation
- $\delta^{18}O$ suggest that fluid was derived from crystallization of younger tonalites

Abstract
Metatonalite and amphibolite from the Taishan region of the Western Shandong Province in the North China Craton record *c.* 2.60 Ga fluid-present partial melting via the breakdown of biotite, plagioclase and quartz to produce peritectic hornblende and anatectic melt. Eight paired leucosome–melanosome samples from metatonalite and three paired samples from amphibolite were investigated to evaluate the composition of the melt. Hornblende, biotite and plagioclase in the leucosomes and hornblende and plagioclase in melanosomes from both rock types have similar compositions. Two leucosome samples from the metatonalite were influenced by the removal of heavy rare earth element-rich hornblende and the accumulation of plagioclase. The other leucosomes are interpreted to represent near initial melt compositions with a minor component of peritectic hornblende and are enriched in Si, Na and Sr and depleted in K, Ca, Ba and Rb relative to melanosomes. The enrichment of Na in the melt is inconsistent with experimental results of fluid-present melting of tonalite, but is broadly consistent with the experimental results of fluid-fluxed melting of amphibolite. The absence of K-feldspar in both rock types is a critical control on the composition of anatectic melt and initial melt compositions were probably similar for both rock types. Leucosomes inherited rare earth element patterns from their sources, which suggests that some trace element diagrams used to infer tectonic settings and depths of melting are not appropriate for reworked components of Archean grey gneisses. Whole-rock $\delta^{18}O$ suggest that the fluids responsible for inducing local melting were derived from the intrusion and crystallization of ~2.60 Ga tonalites and trondhjemites in the Taishan region. One amphibolite sample has a relatively low $\delta^{18}O$ suggestive of interaction with meteoric water or seawater possibly related to crustal extension and asthenosphere upwelling at ~2.60 Ga. Fluid-present partial melting reworked 2.75–2.60 Ga tonalites and amphibolites, generating ~2.60 Ga sodium-rich components of grey gneisses in the Western Shandong Province.

Key words: *migmatite, TTG, Archean, metamorphism, fluid, anatexis*

1. Introduction
Tonalite–trondhjemite–granodiorite (TTG) suites make up the majority of Archean continental crust (Barker and Arth, 1976; Jahn et al., 1981; Condie, 1981). While it is accepted that TTG suites are originally derived from partial melting of mafic precursors (Rollinson, 2006; Moyen and Martin, 2012), many show evidence of metamorphism and anatexis (Moyen and Martin, 2012) that further

differentiates these suites into more evolved continental crust (e.g. Nehring et al. 2009). Given the multiple thermal events documented in many Archean cratons, this leads to a complex association of grey gneisses (c.f. Moyen, 2011) that may reflect both crustal growth and crustal reworking, which is evident from Nd studies of TTG suites (e.g. Whalen et al., 2002; Jahn et al. 2008) and Hf isotope studies in zircon (e.g. Wan et al. 2014b, 2015). Differentiating between these processes is essential for refining models of Archean crustal growth and geodynamics as well as understanding the long-term chemical evolution of the continental crust.

Partial melting of crustal rocks occurs through fluid-absent and fluid-present processes during high-temperature metamorphism (Brown, 2013; Weinberg and Hasalová, 2015). At upper amphibolite and granulite facies conditions, fluid-absent hydrate-breakdown melting of mafic rocks and TTGs generates melt and the anhydrous peritectic products of melting such as garnet, orthopyroxene and clinopyroxene (e.g. Büsch et al., 1974; Clemens, 2006; Brown, 2013). In most cases, this is thought to be the primary mechanism by which the continental crust has chemically differentiated into a depleted lower portion and a complementary enriched upper portion (e.g. Clemens and Watkins, 2001; Brown, 2010, 2013; Clemens and Stevens, 2015).

The influx of an externally derived hydrous fluid into a rock at $P–T$ conditions at or above its wet solidus can also induce partial melting (fluid-present melting; e.g. Weinberg and Hasalová, 2015). While this mechanism of partial melting may not contribute to chemical differentiation at the crustal scale, it is suggested that it can have local impacts on the rheology of the crust during orogenesis (e.g. Mogk, 1992; Berger et al., 2008; Genier et al., 2008; Ward et al., 2008; Reichardt and Weinberg, 2012) and may be particularly important in local internal chemical differentiation of Archean TTG suites (e.g. Mogk, 1992; Nehring et al., 2009; Sawyer, 2010; Lee and Cho, 2013; Morfin et al., 2014; Garcia-Arias et al., 2015; Carvalho et al., 2016). Relatively few studies, however, have investigated reworked TTG suites that are the product of fluid-present partial melting (e.g. Watkins et al., 2007; Clemens et al., 2006), but understanding this process is essential for evaluating crustal reworking of Archean terranes.

Grey gneisses and granites of the Western Shandong Province represent the typical exposure of Neoarchean crustal reworking in the North China Craton. While comprehensive U–Pb ages and Hf isotope data exist from TTGs, amphibolites and granites (e.g. Wan et al. 2014a, b), field and petrographic evidence for partial melting of these rocks have only preliminarily been presented (Ren et al., 2016). This evidence is essential to interpreting the isotopic and geochronological data that exist from the Western Shandong Province and to understand the thermochemical evolution of the North China Craton. In this study, field and petrographic observations are coupled with geochemical analyses to elucidate the processes that contributed to the differentiation of early Neoarchean crust in the Western Shandong Province. The source of the fluids responsible for fluxing partial melting is constrained using whole-rock oxygen isotope analysis, and implications for inferring the depth of melting from trace element concentrations in reworked TTG gneisses is discussed.

2. Regional Geology

The Western Shandong Province is the largest exposure of early Neoarchean crust in the North China Craton (Fig. 1). Protracted Neoarchean magmatism from *c.* 2.75 Ga to 2.5 Ga in the Western Shandong Province was divided by Wan et al. (2014b) into early and late Neoarchean associations, which are separated by a magmatic hiatus from roughly 2.60 to 2.55 Ga.

The Taishan region represents one of the most extensive exposures of early Neoarchean rocks in the Western Shandong Province ('Belt B' of Wan et al. 2010, 2011, 2014a, 2014b) and is dominated by TTG gneisses and amphibolites with a relatively minor amount (~10 vol.%) of supracrustal rocks (Jahn et al., 1988). The oldest exposed unit is the 2.75–2.70 Ga supracrustal Yanlingguan-Liuhang succession, which contains metabasalts and metasedimentary rocks (Wan et al., 2012a). This was intruded by early Neoarchean (*c.* 2.75–2.60 Ga) tonalites and meta-mafic dykes (Ren et al., 2016). Magmatic zircon from early Neoarchean rocks yields εHf_t values that range from ~4 to 10, which suggests that these rocks were

derived from a relatively juvenile source (Wan et al., 2014b) and indicates a major period of crustal growth at this time.

Metamorphism and anatexis at the end of the early Neoarchean association at *c.* 2.63–2.60 Ga is widespread in Belt B (Wan et al., 2014b; Ren et al., 2016). However, metamorphism and anatexis at the end of the late Neoarchean association at *c.* 2.50 Ga is widespread in Belts A and C (Dong et al., 2017) and not Belt B. This is possibly because Belt B remained at higher crustal levels during 2.50 Ga metamorphism (Dong et al., 2017). Trondhjemite dykes and sills are ubiquitous in 2.75–2.60 Ga metatonalites and 2.60 Ga veins are interpreted to have formed as a result of anatexis of older TTGs (Wan et al., 2014b; Ren et al., 2016). $\delta^{18}O$ of zircon between +3.3 and +4.8 ‰ from metamorphic and recrystallized zircon in an early Neoarchean gneissic tonalite suggest the involvement of fluids of meteoric origin possibly related to crustal extension (Ren et al., 2016).

Neoarchean amphibolites and granitoid gneisses are cross-cut by a *c.* 2.55 Ga tonalite as well as 2.5 Ga monzogranite dykes (Wan et al., 2014b; Gao et al., 2018). Peng et al. (2013) suggested that *c.* 2.5 Ga Ba–Sr enriched granites were derived from an enriched mantle source. Alternatively, Wan et al. (2014b) suggested that some of these granites were generated through crustal reworking of early Neoarchean units based on relatively non-radiogenic ϵHf_t values of zircon.

3. Rock types and petrology
3.1 Metatonalite
Metatonalite gneisses make up the majority of the grey gneisses in the Taishan region (Fig. 1). They are variably deformed with a foliation defined by the parallel alignment of biotite and hornblende (Fig. 2a). Metatonalite contains up to 50 vol.% leucosome (relatively light coloured material dominated by quartz and plagioclase). Melanosomes (relatively dark coloured material containing proportionally more ferromagnesian minerals than the leucosome) contain variable amounts of quartz, plagioclase, hornblende and biotite. More than half of the leucosomes in most outcrops have sharp boundaries with the metatonalite and other leucosomes, cross-cut the foliation in the melanosome, and are generally free of ferromagnesian minerals. These leucosomes compose 20–30 vol.% of the outcrop, range from 5 to 30 cm in width (Fig. 2a), and do not contain mafic selvedges. Based on the sharp contacts with the host metatonalite, these are interpreted to represent injected material that may not be sourced locally from partial melting of their host rocks.

A smaller proportion of the total amount of leucosomes have: (1) diffuse boundaries with melanosomes, (2) relatively coarse-grained hornblende compared to host metatonalite (Fig. 2b, c) that contain rounded inclusions of biotite, quartz and plagioclase, and (3) petrographic continuity (similar mineralogy, grain size and modes) with other leucosomes that are concordant with and discordant to the foliation (Fig. 2c, d). Together, these observations are consistent with these leucosomes representing the products of *in situ* partial melting. Leucosome interpreted to be *in situ* are subdivided into two groups: (1) patch leucosomes, which are discordant to the foliation and can occur in isolation (Fig. 2a, b), and (2) stromatic leucosomes, which are concordant with the foliation and commonly connect to discordant patch leucosomes (Fig. 2c, d). Leucosomes range from 1 to 10 cm in width and usually contain coarser-grained hornblende relative to the host melanosome. Neither patch nor stromatic leucosomes contain distinct mafic selvedges along their margins (Fig. 2a–d).

Most metatonalite leucosomes are dominated by approximately equal proportions of quartz and plagioclase as well as relatively coarse-grained subhedral to anhedral poikiloblasts of hornblende (~1–10 vol.%) with rounded inclusions of biotite and minor quartz and plagioclase (Fig. 3a). The inclusions of rounded biotite, quartz and plagioclase in coarse-grained hornblende in the leucosomes are consistent with the simplified partial melting reaction:

biotite + plagioclase + quartz + fluid (H_2O) $\rightarrow$ hornblende + melt   (1)
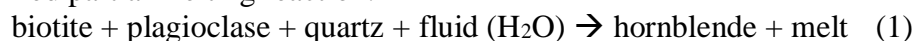
This reaction has been documented in experimental studies (Büsch et al., 1974; Naney, 1983; Gardien et al., 2000) and metaigneous migmatites (Slagstad et al., 2005; Cruciani et al. 2008; Lee and Cho, 2013; Hu et al., 2016).

Melanosomes contain greater proportions of the ferromagnesian minerals (Fig. 3b) and usually contain ~5–10 vol. % hornblende and ~5–20 vol.% biotite, which are generally aligned into a weak foliation. Accessory minerals include epidote, titanite, apatite and zircon. Some leucosomes do not contain coarse-grained hornblende and are dominated by blocky plagioclase with interstitial quartz (Fig. 3c). One 3-mm wide veinlet was observed that contains abundant hornblende that is much coarser than hornblende in the host (Fig. 3d). K-feldspar is absent from the melanosomes and is only found in trace amounts (<1 vol.%) in leucosomes from two samples (T043 and T029A). Epidote and zircon are found in the leucosome and melanosome whereas apatite and titanite appear to be restricted to the melanosomes.

3.2 Amphibolites

Amphibolites are found as metre- to decametre-scale enclaves in metatonalite and range from relatively undeformed and blocky in appearance (Fig. 4a) to strongly deformed and sill-like in appearance (Fig. 4b). Given the pervasive ductile deformation of the amphibolites and the grey gneisses, the primary relationship between them is unclear. Amphibolites contain up to 10 vol.% leucosome and the morphology of these leucosomes is usually patchy to stromatic (Fig. 4c, d). Similar to the metatonalites, the leucosomes can contain coarse-grained hornblende (up to ~20 vol.%) and are dominated by plagioclase (~40–70 vol.%) and quartz (~10–20 vol.%). Coarse-grained hornblende in the leucosomes commonly contains inclusions of biotite (Fig. 3e) and quartz. Amphibolite melanosomes are dominated by hornblende (~30–60 vol.%), biotite (~2–10 vol.%), plagioclase (~10–30 vol.%) and minor quartz (~2–10 vol.%) as well as accessory zircon, titanite, apatite and epidote. No orthopyroxene or clinopyroxene was observed in the leucosomes or melanosomes of the amphibolites.

In general, the amphibolites contain less leucosome (<10 vol.%) than the tonalites. Some leucosomes in the amphibolite are petrographically continuous with leucosome in the host metatonalite (Fig. 4a) and these are interpreted to be injected. These leucosomes have sharp contacts with the amphibolites and cut across the foliation (Fig 4e). However, most leucosomes in the amphibolites are inferred to be *in situ*. Similar to the metatonalite, interpreted *in situ* leucosomes in the amphibolites are characterized by diffuse margins with melanosomes, the presence of coarse-grained hornblende (Fig. 4e, f) and petrographic continuity between discordant and concordant leucosomes.

Leucosomes in amphibolite are similar in composition to the leucosomes in metatonalite and are composed of quartz and plagioclase with coarse-grained poikiloblasts of hornblende with rounded inclusions of biotite and minor quartz and plagioclase (Fig. 3e). Reaction (1) is also interpreted to represent the principal partial melting reaction for the amphibolites.

4. Mineral compositions

4.1 Methods

Samples were collected from outcrop or float beneath freshly blasted outcrop in areas around the Lihang reservoir (Fig. 1). Sampling locations are shown in Table 1. Major element compositions of hornblende, plagioclase, biotite and epidote from four samples (T008A, T043, T008B and T027A) were measured using a JEOL-8200 Electron Microprobe in the Robert M. MacKay Electron Microprobe Laboratory in the Department of Earth Sciences at Dalhousie University. Natural standards were used for calibration. An operating voltage of 15 kV and beam current of 20 nA were used with a ~1 μm beam spot. Data were processed with Probe for EPMA with a ZAF correction scheme. The full dataset is presented in the Supplementary Table S1.

Trace element compositions of hornblende from the same four samples (T008A, T043, T008B and T027A) were targeted for trace element analysis. Hornblende from the melanosome and coarse-

grained (inferred peritectic) hornblende from the leucosomes of both rock types were analyzed. Trace element concentrations were measured in the Metal Isotope and Geochemistry Laboratory at the University of Waterloo using an Analyte G2 193 nm Excimer laser coupled to an Agilent 8800 triple quadrupole ICP-MS (used in single quadrupole mode). The following masses were measured: ^{29}S, ^{31}P, ^{43}Ca, ^{44}Ca, ^{45}Sc, ^{47}Ti, ^{51}V, ^{52}Cr, ^{60}Ni, ^{66}Zn, ^{71}Ga, ^{72}Ge, ^{85}Rb, ^{88}Sr, ^{89}Y, ^{90}Zr, ^{133}Cs, ^{137}Ba, ^{139}La, ^{140}Ce, ^{141}Pr, ^{145}Nd, ^{146}Nd, ^{147}Sm, ^{151}Eu, ^{157}Gd, ^{159}Tb, ^{163}Dy, ^{165}Ho, ^{166}Er, ^{169}Tm, ^{172}Yb, ^{175}Lu, ^{178}Hf, ^{232}Th, ^{238}U. Dwell times were 20 ms except for ^{29}Si, which was 10 ms. The carrier gas was ~1 L/min He with ~1 L/min of Ar added in a mixing bulb between the ablation chamber and the torch. Three cleaning pulses were followed by 30 s of background acquisition and 30 s of ablation with a 7 Hz repetition rate, 4 J/cm^2 energy (measured at sample surface) and a 65 μm spot. NIST612 was used as a primary standard and BCR-2G was monitored as a secondary standard. ^{29}Si was used as an internal standard and analyses were on the same spots measured by electron microprobe. Data was reduced using Iolite 3.6 using the "Trace_Elements_IS" Data Reduction Scheme (Paton et al., 2011). Average trace element concentrations in BCR-2G were within 10% of the accepted values except for Y and Cs, which were within 15%, and Zn and Ge which were outside the accepted values by more than 20%. The full dataset is presented in the Supplementary Table S2 and results for BCR-2G in Table S3. Select compositional information is plotted in Figure 5.

4.2 Results

4.2.1 Metatonalites (T008A and T043).

Hornblende in the melanosome has X_{Mg} (molar Mg / [Fe + Mg]) values of 0.46-0.51 (Fig. 5a), Ti concentrations of 0.03–0.08 atoms per formula unit (a.p.f.u.) (Fig. 5b), and alkali concentrations (Na + K) of 0.50–0.62 a.p.f.u (Fig. 5c). Hornblende in the leucosome has X_{Mg} values of 0.46–0.55, Ti concentrations of 0.03–0.08 a.p.f.u. and alkali concentrations (Na + K) of 0.49–0.63 a.p.f.u, which are all similar to values from the melanosome. Plagioclase in the melanosome have X_{An} (molar Ca / [Ca + Na + K]) values of 0.29–0.34 (Fig. 5d), which is similar to the values of plagioclase in the leucosome (X_{An} = 0.31–0.35). No core–rim zoning was observed in plagioclase from either leucosome or melanosome. Biotite in the melanosome has X_{Mg} values of 0.50–0.56 that are similar to values in the leucosome (0.53–0.59). A single biotite inclusion in hornblende in leucosome has a similar X_{Mg} value of 0.53 (sample T043). Chondrite-normalized rare earth element (REE) patterns of hornblende are variable and there are no systematic changes between the leucosome and melanosome (Fig. 5e). Most hornblende have slightly depleted light REE (LREE), minor to negligible negative Eu anomalies and flat heavy REE (HREE) patterns. Three LREE-depleted hornblende grains are spatially associated with epidote in thin section.

4.2.2. Amphibolites (T008B and T027A)

Hornblende in the melanosome has X_{Mg} values of 0.42–0.55, Ti concentrations of 0.04–0.09 a.p.f.u. and alkali concentrations of 0.54–0.62 a.p.f.u (Fig. 5a-c). Most hornblende in the leucosome has X_{Mg} values of 0.42–0.44 (with one exception of 0.50), which are generally lower than values in the melanosome. Ti concentrations in hornblende in the leucosome range from 0.05 to 0.09 a.p.f.u. and alkali concentrations are 0.54–0.66 a.p.f.u, which are similar to hornblende in the melanosome. Plagioclase in the melanosome has X_{An} values of 0.28–0.32 (Fig. 5d), which is nearly the same range of values of plagioclase in the leucosome (X_{An} = 0.28–0.32). Minor core–rim zoning was found in one plagioclase grain in a leucosome that has a more sodic rim (X_{An} = 0.28) than core (X_{An} = 0.32). Biotite in the melanosome has X_{Mg} values of 0.56–0.58 with one exceptional value of 0.48. These are similar to values of 0.47–0.55 in the leucosome. Biotite inclusions in hornblende in the leucosome have X_{Mg} values of 0.53-0.55. Chondrite-normalized REE patterns of hornblende from the amphibolite show slightly negative Eu anomalies, depleted LREE and flat HREE patterns, and La_N/Yb_N ratios varying from ~1 to

<1 (Fig. 3f). Hornblende in the melanosome has generally slightly lower concentrations of the REE and some have depleted LREE compared with hornblende in leucosome (Fig. 5f).

4.2.3 Comparison
There are no clear differences between the composition of plagioclase in the leucosomes and the melanosomes from the metatonalites and amphibolites. Plagioclase from the amphibolite have slightly lower median X_{An} values of ~0.30 compared with median values of ~0.33 in the metatonalite (Fig. 5d). Hornblende from the amphibolite has slightly lower Si (a.p.f.u) on average than the metatonalite, but there is no substantial difference between the compositions of hornblende found in the leucosome or melanosome of the amphibolite and metatonalite (Fig. 5a–c). Hornblende compositions from both rock types plot along a trajectory between edenite and ferropargasite, with two exceptions from the melanosome in the amphibolite that plot just inside the pargasite field of Leake et al. (1997). Finally, hornblende from the metatonalite and the amphibolites has similar concentrations of the rare earth elements (Fig. 5e–f)

5. Geochemistry
5.1 Methods
Samples range in weight from 1 to 3 kg. Serial sawing was used to obtain portions of leucosome and melanosome from a single sample. In the sample numbers used here and Table 1, "L" as the last character refers to the leucosome component of a paired sample (e.g. T008BL) and "M" to the melanosome component (e.g. T008BM). Leucosome was only sampled when it was interpreted to be *in situ* based on the criteria listed earlier. Melanosome samples are interpreted to represent the closest available composition of the protoliths (e.g. mesosome) although they may have been slightly modified from protolith compositions due to local melt loss or gain. Whole-rock analyses were conducted on 22 samples by ICP-OES for major elements and ICP-MS for trace elements at ActLabs (Ancaster, Ontario, Canada) using their 4LithoResearch package. Rare earth element concentrations were normalized to chondrite using the values from McDonough and Sun (1995).

5.2 Results
Major-element, trace-element and rare earth element data are presented in Supplementary Table S4. The data are divided into the leucosome and melanosome components of the metatonalite and the amphibolite. Patchy and stromatic leucosomes are grouped. Major-element values are summarized as variation diagrams in Figure 6 along with the compositions of ~2.5 Ga granites from Peng et al. (2013) and Wan et al. (2012b). Trace-element plots are shown in Figure 7. Chondrite-normalized rare earth element diagrams are presented in Figures 8–9. Boxplots that show the distribution of the enrichment factors of the leucosomes relative to the melanosomes are shown in Fig. 10 for samples that are interpreted to represent near-initial melt compositions (see Discussion).

　　　　Leucosomes are enriched in SiO_2 relative to the melanosome for both metatonalite and amphibolite (Fig. 6, 10). Concentrations of SiO_2 range from 64 to 74 wt.% for leucosomes from the metatonalite and from 56 to 72 wt.% for leucosomes from the amphibolite (Fig. 6). Leucosomes are also enriched in Na_2O relative to the melanosome for both rock types (Fig. 6, 10). Samples of the metatonalite and amphibolite (leucosome and melanosome components) show negative correlations between SiO_2 and CaO, K_2O, $Fe_2O_{3(T)}$ and MgO. With increasing SiO_2, Al_2O_3 and Na_2O remain relatively constant. Samples of the late K-rich (~4–5 wt.% K_2O) granites from Peng et al. (2013) and Wan et al. (2012b) have much higher concentrations of K_2O than leucosomes in the metatonalite and amphibolite (Fig. 6).

　　　　Concentrations of Sr for both metatonalite and amphibolites are slightly higher in leucosomes compared with melanosomes (Fig. 7a, b, 10). Barium and Rb are generally depleted in the leucosomes relative to melanosomes in both rock types (Fig. 7a,b). Except for two leucosome samples from the

metatonalite, the melanosomes and leucosomes from both rock types yield Sr/Y ratios <100, for a range of Y concentrations from 6 to 27 ppm (Fig. 7c). The two exceptions are leucosome samples T026L and T029L, which have concentrations of Y of ~2 ppm and Sr/Y ratios >200. All samples have La_N/Yb_N (chondrite normalized) ratios between 2 and 55 and show a range of Yb_N values from 1 to 18 (Fig. 7d).

Chondrite-normalized rare earth element patterns from the melanosomes from metatonalite and amphibolite are generally smooth (Fig. 8a, b). Metatonalite sample T028CM displays a small negative europium anomaly (Fig. 8a). Leucosomes have similar chondrite-normalized REE trends and concentrations compared to the melanosomes with two exceptions (Fig. 8a–d). Metatonalite leucosomes samples T026L and T029BL show pronounced positive europium anomalies and low concentrations of the heavy rare earth elements relative to the metatonalite melanosomes (Fig. 8a, b). Metatonalite melanosome T028CM has a steeper enrichment of the LREE relative to the paired leucosome (T028CL).

Metatonalite leucosomes show similar chondrite-normalized trends and similar or lower concentrations of the rare earth elements relative to their paired melanosomes (Fig. 9a–h). Sample T028C has small negative Eu anomalies in both the melanosome and the leucosome (Fig. 9c). Samples T026 and T029B contain leucosomes with pronounced positive Eu anomalies whereas their paired melanosomes contain smooth chondrite-normalized rare earth element profiles. Two paired samples from the amphibolite (T027A and T025A) have similar concentrations of the rare earth elements and similar chondrite-normalized patterns (Fig. 9i,j) whereas leucosome from sample T008B is more depleted in the REE (Fig. 9k).

In summary, leucosomes from both the metatonalite and the amphibolite are enriched in SiO_2, Na_2O and Sr relative to their paired melanosomes (Fig. 10). All other measured elements are enriched in the melanosomes.

6. Stable isotope geochemistry

6.1 Methods

Oxygen-isotope analysis of whole-rock samples was performed at the Laboratory for Stable Isotope Science (LSIS), The University of Western Ontario, London (Ontario), Canada. Approximately 8 mg of sample powder were weighed into spring-loaded sample holders, evacuated overnight at *ca.* 150ºC, and then placed into nickel reaction vessels and heated *in vacuo* at 300ºC for a further 3 hours to ensure removal of surface water. The samples were then reacted overnight at *ca.* 580ºC with ClF_3 to release silicate-bound oxygen (Borthwick and Harmon, 1982 following Clayton and Mayeda, 1963). The oxygen was converted to CO_2 over red-hot graphite for isotopic measurement using a Micromass Optima, dual-inlet, stable-isotope-ratio mass-spectrometer. Results are reported using δ-notation in parts per thousand (‰) relative to Vienna Standard Mean Ocean Water (VSMOW). The $\delta^{18}O$ of laboratory standard CO_2 was +10.13±0.2 ‰ (accepted value = +10.2 ‰). Laboratory standard quartz (n=3) and basalt (n=2) were reproducible to ±0.10 ‰ (n=3) and ±0.13 ‰ (n=2), respectively. Duplicates of samples T008BM, T008CM and T027B yield standard deviations of 0.82, 0.03 and 0.27 ‰, respectively.

6.2 Results

The $\delta^{18}O$ values are reported in Supplementary Table S5 and plotted in Figure 11. With three exceptions, whole-rock $\delta^{18}O$ of leucosomes and melanosomes range from +5.5 to +8.3 ‰, which are within or higher than the range of values of mantle-derived magmas (~+6.0 ± 0.5 ‰; Taylor and Sheppard, 1986). The three exceptions are samples T025AL ($\delta^{18}O$ of +3.2‰), T025AM (+2.6‰), and T027AM (+4.9 ‰), which have lower values than mantle-derived magmas. For paired samples, leucosomes have higher $\delta^{18}O$ than their paired melanosome except for amphibolite samples T025A and T027A (Fig. 11). Leucosome and melanosome from metatonalite samples T025B and T043 have similar $\delta^{18}O$ (Fig. 11).

7. Discussion

7.1 Initial melt compositions

Leucosomes in migmatites may not represent initial (i.e. unmodified) crustal melt compositions. Processes such as fractional crystallization (Sawyer, 1987; Solar and Brown, 2001; Morfin et al., 2014; Carvalho et al., 2016; Fancello et al., 2018) and drainage of fractionated melt (e.g. Brown et al., 2016; Wolfram et al., 2017) can modify the compositions of *in situ* leucosome. Feldspar fractionation is an important control on the major and trace element compositions of melt and can be identified using the presence or absence of Eu anomalies relative to the starting material (e.g. Sawyer, 1987).

For two paired samples in the metatonalite (T026, T029B), the leucosomes have pronounced positive Eu anomalies and relatively low REE concentrations compared with their melanosomes (Fig. 9). These two leucosomes were sampled from stromatic leucosome, and have coarse, interlocking plagioclase with interstitial quartz (Fig. 3c). These leucosome samples are interpreted to represent compositions modified through the accumulation of early-crystallized plagioclase (e.g. Sawyer, 1987; Slagstad et al., 2005), possibly due to filter pressing (c.f. Brown et al., 1995), with the extraction of complementary fractionated melt (e.g. Brown et al., 2016).

Samples T026L and T029BL have elevated Sr/Y ratios and they plot in the 'adakite' field defined by Defant and Drummond (1990) in the Sr/Y–Y diagram (Fig. 7c). These samples also have relatively high La_N/Yb_N ratios relative to the other leucosomes and the lowest Yb concentrations (Fig. 7d), which is also commonly used as a characteristic of adakitic affinities and restitic garnet in the source rocks (see discussion in Moyen, 2009). The measured low concentrations of HREE in the leucosome, however, developed in the absence of garnet in the source for the metatonalite. A similar conclusion was reached by Wang et al. (2013) for samples from the North Dabie Terrane, where leucosomes that plot in 'adakitic' fields in La_N/Yb_N–Yb_N and Sr/Y–Y diagrams were interpreted to have formed through fluid-present partial melting of quartzofeldspathic gneisses with restitic hornblende in the middle crust, without garnet in the source rocks.

The relatively depleted HREE composition of these two samples (T026L and T029BL) from the Taishan region is possibly due to the removal of peritectic HREE-rich hornblende (e.g. Reichardt and Weinberg, 2012). The presence of leucosome with no coarse-grained peritectic hornblende (e.g. Fig. 2d) and veinlets with possible cumulates of coarse-grained peritectic hornblende (Fig. 3d) are compatible with the physical removal of peritectic hornblende from migrating melt. A simple mass balance adding weight fractions of hornblende (using the average REE concentrations of hornblende from leucosomes in metatonalites in this study) to the composition of T026L is shown in Figure 12. The addition of 5–20 wt.% hornblende results in similar concentrations of the HREE for the complementary melanosome (T026M) and similar HREE concentrations to leucosomes from other metatonalites (Fig. 12). For example, the addition of 10 wt.% hornblende to T026L results in a La_N/Yb_N ratio of 5 and a Yb_N value of 6, which plot outside the 'adakite' field and close to the other metatonalite leucosome compositions in Figure 7d. Therefore, low HREE concentrations in reworked grey gneisses may not be diagnostic of garnet in the source, and consequently, such HREE concentrations are not necessarily a proxy for depth of melting.

The remaining paired samples from the metatonalite and all paired samples from the amphibolite have leucosomes and melanosomes with similar chondrite-normalized REE patterns (Fig. 9). These measured leucosome compositions are likely a combination of former melt (now represented by quartz and plagioclase) as well as a minor component of peritectic hornblende that is suggested by the model in Figure 12. For the amphibolites, hornblende fractionation may be hard to resolve due to the similar chondrite-normalized profiles and values of the REE between hornblende (Fig. 5f) and whole-rock samples (Fig. 9). Measured leucosome compositions from the amphibolite and leucosome compositions without strong Eu anomalies from the metatonalite (i.e. excluding samples T026L and T029BL) are interpreted to represent the represent the closest approximations to unmodified initial melt based on the absence of strong Eu anomalies in leucosomes that would indicate significant feldspar fractionation or

accumulation (e.g. Sawyer, 1987). These leucosomes compositions are used to investigate the composition of melt generated through fluid-present partial melting of metatonalite and amphibolite.

The composition of the interpreted near initial melt compositions and the results of experimental melting studies for fluid-present systems are summarized in Figure 13. In Figure 13a, leucosome compositions plot towards the Na+Ca apex away from the melanosome compositions and away from the Fe+Mg+Ti apex. The closest compositional matches of experimental starting materials to the metatonalite from the Western Shandong Province are tonalites from Watkins et al. (2007). The closest compositional matches to the amphibolites are mafic rocks from Beard and Lofgren (1991) and Winther (1996).

The melt compositions from fluid-present melting of a tonalite from Watkins et al. (2007) plot towards the potassium apex in Figure 13a and towards the normative orthoclase apex in Figure 13b away from the starting compositions, which is opposite to the trend observed in the leucosomes from this study. The divergent trends of melt compositions may relate to the starting composition and the fluid-present partial melting reactions. In the experiments, K-feldspar was consumed during the initial stages of congruent fluid-present melting and biotite and hornblende remained stable (Watkins et al., 2007). Most of the melt was generated during the breakdown of K-feldspar and resulted in relatively K-rich glass compositions (Fig. 13a, b). In metatonalite samples from the Taishan region, K-feldspar was only observed in the leucosome of two metatonalite samples (T043 and T029A; K-feldspar is <1 vol.% of these samples). Because of the paucity of K-feldspar, the potassium budget in the metatonalite samples was likely controlled by the breakdown of biotite and some of the released potassium was partitioned into growing peritectic hornblende that may or may not have been physically separated from the melt (Fig. 3c, d). The compositions of the melt were therefore dominated by the breakdown of quartz and plagioclase as well as biotite, which is supported by the elevated concentrations of SiO_2, Na_2O and Sr in the leucosomes compared with the melanosomes (Fig. 10). We speculate that the absence (or very low mode) of K-feldspar in the protoliths of the metatonalites from the Taishan region resulted in melt with very low concentrations of K (Fig. 13a, b) relative to the glass compositions of the H_2O-saturated experimental runs of Watkins et al. (2007).

Glass compositions from fluid-present melting of amphibolites from Beard and Lofgren (1991) and Winther (1996) plot towards the Na+Ca apex in Figure 13a, which is broadly consistent with the measured leucosome compositions from the Taishan amphibolites. Normative feldspar modes of leucosomes from the amphibolites are also consistent with the results from Beard and Lofgren (1991) but normative modes of melt compositions from Winther (1996) are more anorthite-rich (Fig. 13b). In general, the measured compositions of leucosomes in amphibolite are broadly consistent with experimental results and are also similar to the leucosome compositions from the metatonalite.

The two very different rock types investigated in this study (amphibolites and metatonalites) have different melanosome compositions but similar leucosome compositions (Figs 6, 8, 13). In addition, hornblende and plagioclase compositions are similar between migmatite components (leucosome and melanosome) as well as between rock types (Fig. 5). The similar mineral compositions suggests that the amphibolites and metatonalites experienced the same general partial melting reaction that included the breakdown of quartz, plagioclase and biotite in the presence of H_2O to produce melt and hornblende. Because of the high abundance of all of the mineral reactants (with similar compositions) in both rock types, the same reaction could have proceeded in the metatonalite and amphibolite generating similar melt compositions (Fig. 13). We speculate that the scarcity of K-feldspar in metatonalites from the Taishan region may be a critical factor in controlling melt composition and why the two different rock types yielded similar leucosome compositions.

The generation of more sodium-rich and less potassium-rich melt compositions relative to their sources documented in this study is the opposite to most modern crustal differentiation trends (e.g. Lameyre and Bowden, 1982) and the evolution of some reworked TTG suites (Jébrak and Harnois, 1991). Furthermore, most TTG suites do not show clear differentiation trends among Na, Ca and K

(Moyen and Martin, 2012). Trends towards more sodium-rich compositions, however, have been observed in the western Gyeonggi Massif in Korea (Lee and Cho, 2013), the Dabie Mountains in Eastern China (Hu et al., 2016), and in the Pilbara craton (Collins, 1993).

Sodium-rich components of TTG suites (including trondhjemites) are generally interpreted to record relatively high-pressure (e.g. Moyen and Martin, 2012) and high-temperature melting of mafic rocks (Palin et al., 2016). The results of Lee and Cho (2013), Hu et al. (2016) and this study, however, suggest that these components may represent relatively low-pressure melts produced during fluid-present anatexis (Fig. 14). Fluid-present partial melting of oceanic gabbros also generates sodium-rich plagiogranites at low pressures (e.g. Koepke et al., 2004). In addition, Johnston and Wyllie (1988) noted that secondary trondhjemites derived from partial melting of pre-existing tonalites and trondhjemites inherit their trace element concentrations, including highly negative slope on chondrite-normalized REE plots. These authors also suggest that REE abundances should be higher in the second-generation melts, which contrasts with most of leucosome samples from the Taishan region, which have lower concentrations of the REE than their paired melanosomes (Fig. 9, 10). Nonetheless, reworking of grey gneisses may yield melt compositions that have similar La_N/Yb_N ratios to their sources. For seven out of eleven paired samples in this study, the leucosomes contain higher La_N/Yb_N ratios than their paired melanosomes for both metatonalite and amphibolite. This is important because these inherited values in reworked grey gneisses should not be used to infer the depth and the geodynamic setting of partial melting. In addition, the removal or entrainment of HREE-rich hornblende will also impact the La_N/Yb_N ratio of the magma (e.g. Fig. 12).

7.2 Source of fluid
Except for amphibolite sample T025A, samples from the Taishan region have whole-rock $\delta^{18}O$ compositions similar to grey gneisses and amphibolites from other Archean terranes (e.g. Longstaffe and Schwarcz, 1977; Longstaffe, 1979; Longstaffe and Gower, 1983; Whalen et al., 2002). The higher $\delta^{18}O$ of leucosomes compared with paired melanosomes (Fig. 9) likely reflects the preferential partitioning of ^{18}O into quartz and feldspar (the dominant components of the leucosomes) compared with ferromagnesian minerals, such as biotite and hornblende (e.g. Taylor and Epstein, 1962) that are in higher proportions in the melanosome. This also reflects the general crustal differentiation trend towards higher $\delta^{18}O$ in more evolved magmas (e.g. Eiler, 2001). The $\delta^{18}O$ of all metatonalite samples and amphibolite samples T008B and T027AL are the same as or higher than the mantle (~6.0 ± 0.5 ‰; Taylor and Sheppard, 1986), which is consistent with internal differentiation and the absence of interaction with heated meteoric water or seawater. Sample T027AM has a $\delta^{18}O$ slightly lower than the mantle, but it is not substantially different.

A probable source for externally-derived H_2O that induced melting in the Taishan migmatites are contemporaneous (~2.60 Ga) intrusive tonalites and trondhjemites present throughout the region (Wan et al., 2014b). Two grey gneisses investigated by Ren et al. (2016) have U–Pb zircon crystallization ages of *c.* 2.64 Ga and zircon metamorphic ages of 2.63–2.60 Ga (Ren et al., 2016). This suggests that there may have been reworking of both older (*c.* 2.70 Ga) and younger (*c.* 2.64 Ga) gneisses through fluid-present partial melting at *c.* 2.60 Ga.

Although these voluminous *c.* 2.6 Ga tonalites and trondhjemites were likely generated at depth due to higher-temperature hydrate-breakdown melting reactions, their transit through shallower crust— now the exposed crustal level in the Taishan region—may have brought in H_2O that reworked older tonalites and amphibolites. Two proposed mechanisms for the transfer of H_2O from a magma to the surrounding wall rock to induce partial melting are: (1) the development of a strong activity gradient between an intruding magma with high H_2O activities with the host subsolidus rock with lower H_2O activities (e.g. Weinberg and Hasalová, 2015), or (2) crystallization of intruding magmas and release of H_2O into the surrounding rocks (e.g. Finger and Clemens, 1995; Annen and Sparks, 2002). The timescales of H_2O diffusion into the wall rock will compete with the duration of magma ascent through

the crust. Vertical magma ascent through the crust is estimated to be as fast as years (Petford et al., 2000), which is much faster than the timescales of H_2O diffusion through the magma due to the relatively slow diffusivity of H_2O in silicate liquids (c.f. Nowak and Behrens, 1997). The duration of magma ascent may be longer, which may induce local melting next to the vertical ascent conduits. However, the paucity of dykes at a high angle to the foliation (Figs 2, 4) in the Taishan migmatites suggests that H_2O diffusion into the wallrock during magma ascent may not have been the dominant mechanism of H_2O transfer.

Alternatively, the emplacement of magmas derived from deeper in the crust may result in higher H_2O activities than the wallrock during cooling and crystallization of anhydrous minerals. Considering that many of the injected leucosomes are found at a low angle to the dominant fabric (Figs 2 and 4), these probably do not represent former vertical magma ascent conduits but rather zones of local dilation and magma accumulation. Furthermore, the paucity of hydrous minerals in (e.g. hornblende, biotite) and lack of mafic selvedges around leucosomes (Figs 2a, 3e) in the Taishan migmatites is consistent with the efficient transfer of H_2O from the magma into the surrounding wall rock (e.g. White and Powell, 2010). Therefore, exsolved H_2O from the crystallization of injected tonalites and trondhjemites is the most probable cause of fluid-present melting of the surrounding metatonalites and amphibolites.

One amphibolite sample (T025A) has a leucosome and melanosome with $\delta^{18}O$ lower than the mantle, which are also too low to be derived solely from igneous processes and suggests some interaction with a low-^{18}O reservoir. The isotopic composition of these samples may reflect that of their (hydrothermally altered) protoliths or interaction with a low-^{18}O fluid during partial melting.

Whether the protolith to the amphibolite is intrusive into TTG country rock or supracrustal in origin and entrained into TTG magmas is unclear due to strong deformation and recrystallization during metamorphism in the Taishan region. Amphibolites in the Western Shandong Province may represent fragments of the supracrustal component of the Yanlingguan-Liuhang succession (Wan et al., 2012a) or may be intrusive in origin. If the amphibolites are of supracrustal origin, the low $\delta^{18}O$ may reflect hydrothermal alteration of the protoliths. The sharp contacts of the amphibolites with the host tonalite and the lack of compositional layering (other than leucosome) are suggestive of an intrusive origin. Amphibolites in the Yanlingguan-Liuhang succession commonly show layering and some have pillow structures (e.g. Wan et al., 2014b) indicative of a volcanic protolith, which are not observed in the amphibolites enclaves. Therefore, the balance of evidence suggests that the amphibolites are of intrusive origin, but we cannot rule out the possibility that some may be enclaves of supracrustal material assimilated into the TTGs during ascent or emplacement.

If the amphibolites are intrusive in origin, then there are several possible explanations for the low $\delta^{18}O$ from three samples (T025AL, T025AM and T027AM). Taylor and Sheppard (1986) outlined three mechanisms that can generate primary magmas with low $\delta^{18}O$, including: (1) anatexis of $\delta^{18}O$-depleted source rock, (2) isotope exchange between hydrothermally altered country rock and the magma, and (3) influx of a fluid with low $\delta^{18}O$ into the magma. Anatexis of $\delta^{18}O$-depleted source rock is unlikely since the possible intrusive protoliths of the amphibolites would be derived from the mantle, which has a relatively uniform $\delta^{18}O$ (+6.0 ± 0.5‰; Taylor and Sheppard, 1986). Isotope exchange between the hydrothermally altered country rock (TTGs) and the amphibolites is also unlikely since the host TTGs do not display low $\delta^{18}O$ (Fig. 11). Considering that none of the mechanisms responsible for generating low $\delta^{18}O$ magmas are appropriate for the possible protoliths of the amphibolites in the Taishan region, we interpret the $\delta^{18}O$ of sample T025A to represent interaction with a low-^{18}O fluid during fluid-present partial melting. Longstaffe (1979) reported similar exchange affecting migmatitic gneisses from the Archean Superior Province.

The fluid responsible for fluxing melting of low-$\delta^{18}O$ samples may have been derived from a low-^{18}O reservoir such as seawater or meteoric water (≤0 ‰). Other sources of fluid, such as magmatic or metamorphic fluid, are expected to have $\delta^{18}O$ greater than +5.5‰. Ren et al. (2016) measured $\delta^{18}O$ in zircon and found one sample of metatonalite from the Taishan region to contain c. 2.6 Ga metamorphic

zircon with low δ^{18}O (+1.1 to +3.2‰). These authors suggested that these zircons record meteoric water (or seawater) percolation down crustal-scale faults during crustal extension and asthenosphere upwelling. Crustal extension is also compatible with relatively radiogenic (i.e. juvenile) Hf isotope ratios in $c.$ 2.60 Ga granitoids as well as coeval ultramafic magmatism in the Western Shandong Province (Wan et al., 2014a) The results for amphibolite sample T025A also suggest interaction between low-^{18}O fluid and rocks in the Taishan region and we speculate that this may be related to the same event. The dominant source of fluids, however, is expected to be the crystallization of ~2.60 Ga intrusions that are common amongst the metatonalites and amphibolites in the Taishan region.

7.3 Source of ~2.5 Ga granites in the Western Shandong Province
Late Neoarchean ($c.$ 2.5 Ga) granite plutons in the Western Shandong Province have been proposed to be derived from one of two sources: (1) reworking of Early Neoarchean crust (Wan et al., 2014a) or (2) metasomatized lithospheric mantle above a putative subduction zone (Peng et al., 2013). Wan et al. (2014a) demonstrated that the Hf isotope compositions of zircon from these granites are consistent with derivation from a $c.$ 2.7 Ga (early Neoarchean) juvenile source, which may be the same source that generated the 2.6 Ga tonalites. Peng et al. (2013) suggested an enriched mantle lithosphere source based primarily on trace element concentrations in the granites.

The results of this study suggest that fluid-present melting of Early Neoarchean metatonalite does not produce melt compositions that are potassic enough to generate the late Neoarchean (~2.5 Ga) granite suite in the Western Shandong Province. This does not preclude the possibility, however, that at deeper levels of the crust that a similar metatonalite and amphibolite underwent late Neoarchean fluid-absent hydrate-breakdown melting due to higher temperatures. The experimental study of Watkins et al. (2007) suggests that even fluid-absent melting of tonalites cannot produce compositions that approximate the young K-rich granites that are common in Archean grey gneiss terranes. Extreme fractionation of tonalitic magma may result in more potassic compositions, but the absence of complementary ~2.5 Ga tonalites in the Western Shandong Province suggests that this scenario is unlikely.

8. Conclusions
Fluid-present partial melting at ~2.60 Ga reworked early Neoarchean metatonalites and amphibolites in the Western Shandong Province. Most leucosomes in metatonalites are interpreted to represent near-initial melt compositions (with a minor component of peritectic hornblende) that are enriched in sodium compared with their melanosomes and yield chondrite-normalized REE slopes that are similar to those from their paired melanosomes, which suggests these patterns are inherited from their source rocks. Some leucosomes have positive Eu anomalies and low concentrations of the HREE, which is interpreted to reflect the accumulation of early-crystallized plagioclase and separation of peritectic hornblende from melt. Reactant minerals in the melanosomes (plagioclase, biotite) and product minerals in the leucosomes (hornblende, plagioclase) also have similar compositions. In addition, amphibolites and metatonalites have leucosomes with similar major and trace element compositions, which suggests that these two different rock types underwent similar partial melting reactions and generated comparable melt and peritectic mineral compositions. The δ^{18}O of leucosomes and melanosomes are consistent with fluid being derived from tonalite and trondhjemite intrusions contemporaneous with metamorphism and partial melting at $c.$ 2.60 Ga. The δ^{18}O of two amphibolite samples suggest interaction with a low-^{18}O fluid (meteoric water?), which may reflect crustal-scale extensional tectonics at $c.$ 2.60 Ga in the Western Shandong Province. Late Neoarchean granites are not related to fluid-present partial melting of 2.7 Ga granitoid rocks.

References
Annen, C., Sparks, R.S.J., 2002. Effects of repetitive emplacement of basaltic intrusions on thermal evolution and melt generation in the crust. Earth Planetary Science Letters 203, 937–955.

Barker, F., 1979. Trondhjemite: definition, environment and hypotheses of origin, in: Barker, F. (Ed.), Trondhjemites, Dacites and Related Rocks, Developments in Petrology Series #6, Elsevier Scientific Publishing Co., Amsterdam, pp. 1–12.

Barker, F., Arth, J.G., 1976. Generation of trondhjemitic-tonalitic liquids and Archean bimodal trondhjemite-basalt suites. Geology 4, 596–600.

Beard, J.S., Lofgren, G.E., 1991. Dehydration melting and water-saturated melting of basaltic and andesitic greenstones and amphibolites at 1, 3, and 6. 9 kb. Journal of Petrology 32, 365–401.

Berger, A., Burri, T., Alt-Epping, P., Engi, M., 2008. Tectonically controlled fluid flow and water-assisted melting in the middle crust: An example from the Central Alps. Lithos 102, 598–615.

Borthwick, J., Harmon, R.S., 1982. A note regarding CIF_3 as an alternative to BrF_5 for oxygen isotope analysis. Geochimca et Cosmochimca Acta 46, 1665–1668.

Brown, C.R., Yakymchuk, C., Brown, M., Fanning, C.M., Korhonen, F.J., Piccoli, P.M., Siddoway, C.S., 2016. From source to sink: petrogenesis of Cretaceous anatectic granites from the Fosdick Migmatite–Granite Complex, West Antarctica. Journal of Petrology 57, 1241–1278.

Brown, M., 2010. Melting of the continental crust during orogenesis: the thermal, rheological, and compositional consequences of melt transport from lower to upper continental crust. Canadian Journal of Earth Sciences 47, 655–694.

Brown, M., 2013. Granite: From genesis to emplacement. Geological Society of America Bulletin 125, 1079–1113.

Brown, M., Averkin, Y.A., McLellan, E.L., Sawyer, E.W., 1995. Melt segregation in migmatites. Journal of Geophysical Research B: Solid Earth 100, 15655–15679.

Büsch, W., Schneider, G., Mehnert, K., 1974. Initial melting at grain boundaries. Part II: Melting in rocks of granodioritic, quartzdioritic and tonalitic composition. Neues Jahrbuch für Mineralogie, Monatshefte 8, 345–370.

Cao, G.O.,1996. Early Precambrian geology of western Shandong. Geol. Publ. House, Beijing, 1–210.

Carvalho, B.B., Sawyer, E.W. and Janasi, V.A., 2016. Crustal reworking in a shear zone: transformation of metagranite to migmatite. Journal of Metamorphic Geology, 34, 237–264.

Clayton, R.N., Mayeda, T.K., 1963. The use of bromine pentafluoride in the extraction of oxygen from oxides and silicates for isotopic analysis. Geochimica et Cosmochimca Acta 27, 43–52.

Clemens, J.D., Yearron, L.M., Stevens, G., 2006. Barberton (South Africa) TTG magmas: Geochemical and experimental constraints on source-rock petrology, pressure of formation and tectonic setting. Precambrian Research 151, 53–78.

Clemens, J.D., 2006. Melting of the continental crust: fluid regimes, melting reactions, and source-rock fertility. in: Brown, M. and Rushmer, T. (Eds.), Evolution and Differentiation of the Continental Crust. Cambridge University Press, Cambridge, pp. 297–331.

Clemens, J., Watkins, J., 2001. The fluid regime of high-temperature metamorphism during granitoid magma genesis. Contributions to Mineralogy and Petrology 140, 600–606.

Clemens, J.D., Stevens, G., 2015. Comment on 'Water-fluxed melting of the continental crust: A review' by RF Weinberg and P. Hasalová. Lithos 234, 100–101.

Collins, W.J., 1993. Melting of Archaean sialic crust under high aH2O conditions: genesis of 3300 Ma Na-rich granitoids in the Mount Edgar Batholith, Pilbara Block, Western Australia. Precambrian Research 60, 151–174.

Condie, K.C., 1981. Archean greenstone belts. *Developments in Precambrian Geology 3.* Elsevier, New York.

Cruciani, G., Franceschelli, M., Jung, S., Puxeddu, M., Utzeri, D., 2008. Amphibole-bearing migmatites from the Variscan Belt of NE Sardinia, Italy: Partial melting of mid-Ordovician igneous sources. Lithos 105, 208–224.

Defant, M.J., Drummond, M.S., 1990. Derivation of some modern arc magmas by melting of young subducted lithosphere. Nature 347, 662–665.

Dong, C., Xie, H., Kröner, A., Wang, S., Liu, S., Xie, S., Song, Z., Ma, M., Liu, D. and Wan, Y., 2017. The complexities of zircon crystllazition and overprinting during metamorphism and anatexis: An example from the late Archean TTG terrane of western Shandong Province, China. Precambrian Research, 300, 181–200.

Eiler, J.M., 2001. Oxygen Isotope Variations of Basaltic Lavas and Upper Mantle Rocks. Reviews in Mineralogy & Geochemistry 43, 319–364.

Fancello, D., Cruciani, G., Franceschelli, M., Massonne, H.-J., 2018, Trondhjemitic leucosomes in paragneisses from NE Sardinia: Geochemistry and P-T conditions of melting and crystallization. Lithos 304–307, 501–517.

Finger, F., Clemens, J.D., 1995. Migmatization and "secondary" granitic magmas: effects of emplacement and crystallization of "primary" granitoids in Southern Bohemia, Austria. Contributions to Mineralogy and Petrology 120, 311–326.

Gao, L., Liu, S., Sun, G., Guo, R., Hu, Y., Fu, J., Wang, M., Ma, C. and Hu, F., 2018. Petrogenesis of late Neoarchean high-K granitoids in the Western Shandong terrane, North China Craton, and their implications for crust-mantle interactions. Precambrian Research 315, 138–161.

García-Arias, M., Corretgé, L.G., Fernández, C., Castro, A., 2015. Water-present melting in the middle crust: The case of the Ollo de Sapo gneiss in the Iberian Massif (Spain). Chemcial Geology 419, 176–191.

Gardien, V., Thompson, A.B., Ulmer, P., 2000. Melting of biotite + plagioclase + quartz gneisses: the role of H_2O in the stability of amphibole. Journal of Petrology 41, 651–666.

Genier, F., Bussy, F., Epard, J.-L., Baumgartner, L., 2008. Water-assisted migmatization of metagraywackes in a Variscan shear zone, Aiguilles-Rouges massif, western Alps. Lithos 102, 575–597.

Hu, Z.P., Zhang, Y.S., Hu, R., Wang, J., Siebel, W., Chen, F., 2016. Amphibole-bearing migmatite in North Dabie, eastern China: Water-fluxed melting of the orogenic crust. Journal of Asian Earth Sciences 125, 100–116.

Jahn, B.M., Glikson, A.Y., Peucat, J.J., Hickman, A.H., 1981. REE geochemistry and isotopic data of Archean silicic volcanics and granitoids from the Pilbara Block, Western Australia: implications for the early crustal evolution. Geochimica et Cosmochimca Acta 45, 1633–1652.

Jahn, B.M., Auvray, B., Shen, Q.H., Liu, D.Y., Zhang, Z.Q., Dong, Y.J., Ye, X.J., Zhang, Q.Z., Cornichet, J., Mace, J., 1988. Archean crustal evolution in China: The Taishan complex, and evidence for juvenile crustal addition from long-term depleted mantle. Precambrian Research 38, 381–403.

Jahn, B.M., Liu, D.Y., Wan, Y.S,, Song, B., Wu, J.S., 2008. Archean crustal evolution of the Jiaodong Peninsula, China, as revealed by zircon SHRIMP geochronology, elemental and Nd-isotope geochemistry. American Journal of Science 308, 232–269.

Jébrak, M., Harnois, L., 1991. Two-stage evolution in an Archean tonalite suite: the Taschereau stock, Abitibi (Quebec, Canada). Canadian Journal of Earth Sciences 28, 172–183.

Johnston, A.D., Wyllie, P.J., 1988. Constraints on the origin of Archean trondhjemites based on phase relationships of Nûk gneiss with H_2O at 15 kbar. Conributions to Mineralogy and Petrology 100, 35–46.

Koepke, J., Feig, S.T., Snow, J., Freise, M., 2004. Petrogenesis of oceanic plagiogranites by partial melting of gabbros: an experimental study. Contributions to Mineralogy and Petrology 146, 414–432.

Lameyre, J., Bowden, P., 1982. Plutonic rock types series: discrimination of various granitoid series and related rocks. Journal of Volcanology and Geothermal Research 14, 169–186.

Leake, B.E., Woolley, A.R., Arps, C.E., Birch, W.D., Gilbert, M.C., Grice, J.D., Hawthorne, F.C., Kato, A., Kisch, H.J., Krivovichev, V.G. and Linthout, K., 1997. Report. Nomenclature of amphiboles: report of the subcommittee on amphiboles of the international mineralogical association commission on new minerals and mineral names. Mineralogical Magazine 61, 295–321.

Lee, Y., Cho, M., 2013. Fluid-present disequilibrium melting in Neoarchean arc-related migmatites of Daeijak Island, western Gyeonggi Massif, Korea. Lithos 179, 249–262.

Longstaffe, F.J., 1979. The oxygen isotope geochemistry of Archean granitoids, in: Barker, F. (Ed.). Trondhjemites, Dacites and Related Rocks. Developments in Petrology Series #6, Elsevier Scientific Publishing Co., Amsterdam, pp. 363–399.

Longstaffe, F.J., Schwarcz, H.P., 1977. $^{18}O/^{16}O$ of Archean clastic metasedimentary rocks: a petrogenetic indicator for Archean gneisses? Geochimca et Cosmochimca Acta 41, 1303–1312.

Longstaffe, F.J., Gower, C.F., 1983. Oxygen-isotope geochemistry of Archean granitoid gneisses and related rocks in the English River Subprovince, northwestern Ontario. Precambrian Research 22, 203–218.

McDonough, W.F., Sun, S-S., 1995. The composition of the Earth. Chemical Geology 120, 223–253.

Mogk, D.W., 1992. Ductile shearing and migmatization at mid-crustal levels in an Archaean high-grade gneiss belt, northern Gallatin Range, Montana, USA. Journal of Metamorphic geology 10, 427–438.

Morfin, S., Sawyer, E.W., Bandyayera, D., 2014. The geochemical signature of a felsic injection complex in the continental crust: Opinaca Subprovince, Quebec. Lithos 196–197, 339–355.

Moyen, J.-F., 2009. High Sr/Y and La/Yb ratios: The meaning of the "adakitic signature". Lithos 112, 556–574.

Moyen, J.-F., 2011. The composite Archaean grey gneisses: Petrological significance, and evidence for a non-unique tectonic setting for Archaean crustal growth. Lithos 123, 21–36.

Moyen, J.-F., Martin, H., 2012. Forty years of TTG research. Lithos 148, 312–336.

Naney, M.T., 1983. Phase equilibria of rock-forming ferromagnesian silicates in granitic systems. American Journal of Science 283, 993–1033.

Nehring, F., Foley, S.F., Hölttä, P., Van Den Kerkhof, A.M., 2009. Internal differentiation of the Archean continental crust: Fluid-controlled partial melting of granulites and TTG–amphibolite associations in central Finland. Journal of Petrology 50, 3–35.

Nowak, M., Behrens, H., 1997. An experimental investigation on diffusion of water in haplogranitic melts. Contributions to Mineralogy and Petrology 126, 365–376.

Palin, R.M., White, R.W., Green, E.C.R., Diener, J.F.A., Powell, R., Holland, T.J.B., 2016. High-grade metamorphism and partial melting of basic and intermediate rocks. Journal of Metamorphic Geology 34, 871–892.

Paton, C., Hellstrom, J., Paul, B., Woodhead, J. and Hergt, J., 2011. Iolite: Freeware for the visualisation and processing of mass spectrometric data. Journal of Analytical Atomic Spectrometry 26, 2508–2518.

Peng, T., Wilde, S.A., Fan, W., Peng, B., 2013. Late Neoarchean potassic high Ba–Sr granites in the Taishan granite–greenstone terrane: Petrogenesis and implications for continental crustal evolution. Chemical Geology 344, 23–41.

Petford, N., Cruden, A., McCaffrey, K., Vigneresse, J.-L., 2000. Granite magma formation, transport and emplacement in the Earth's crust. Nature 408, 669–673.

Reichardt, H., Weinberg, R.F., 2012. Hornblende chemistry in meta- and diatexites and its retention in the source of leucogranites: An example from the Karakoram shear zone, NW India. Journal of Petrology 53, 1287–1318.

Ren, P., Xie, H., Wang, S., Nutman, A., Dong, C., Liu, S., Xie, S., Che, X., Song, Z., Ma, M., Liu, D., Wan, Y., 2016. A ca. 2.60 Ga tectono-thermal event in Western Shandong Province, North China Craton from zircon U–Pb–O isotopic evidence: Plume or convergent plate boundary process. Precambrian Research 281, 236–252.

Rollinson, H., 2006. Crustal generation in the Archean, in: Brown, M. and Rushmer, T. (Eds.). Evolution and Differentiation of the Continental Crust. Cambridge University Press, Cambridge, pp. 173–230.

Sawyer, E.W., 1987. The role of partial melting and fractional crystallization in determining discordant migmatite leucosome compositions. Journal of Petrology 28, 445–473.

Sawyer, E.W., 2010. Migmatites formed by water-fluxed partial melting of a leucogranodiorite protolith: Microstructures in the residual rocks and source of the fluid. Lithos 116, 273–286.

Slagstad, T., Jamieson, R.A., Culshaw, N.G., 2005. Formation, crystallization, and migration of melt in the mid-orogenic crust: Muskoka domain migmatites, Grenville Province, Ontario. Journal of Petrology 46, 893–919.

Solar, G.S., Brown, M., 2001. Petrogenesis of migmatites in Maine, USA: Possible source of peraluminous leucogranite in plutons? Journal of Petrology 42, 789–823.

Taylor, H.P., Epstein, S., 1962. Relationship between O^{18}/O^{16} ratios in coexisting minerals of igneous and metamorphic rocks: part 1: Principles and experimental results. Geological Society of American Bulletin 73, 461–480.

Taylor, H.P., Sheppard, S.M., 1986. Igneous rocks; I, Processes of isotopic fractionation and isotope systematics. Reviews in Mineralogy and Geochemistry 16, 227–271.

Wan, Y.S., Liu, D.Y., Wang, S.J., Dong, C.Y., Yang, E.X., Wang, W., Zhou, H.Y., Ning, Z.G., Du, L.L., Yin, X.Y., Xie, H.Q., Ma, M.Z., 2010. Juvenile magmatism and crustal recycling at the end of the Neoarchean in Western Shandong Province, North China Craton: Evidence from SHRIMP zircon dating. American Journal of Sciences 310, 1503–1552.

Wan, Y.S., Liu, D.Y., Wang, S.J., Yang, E.X., Wang, W., Dong, C.Y., Zhou, H.Y., Du, L.L., Yang, Y.H., Diwu, C.R., 2011. ~2.7 Ga juvenile crust formation in the North China Craton (Taishan-Xintai area, western Shandong Province): Further evidence of an understated event from U–Pb dating and Hf isotopic composition of zircon. Precambrian Research 186, 169–180.

Wan, Y.S., Wang, S.J., Liu, D.Y., Wang, W., Kröner, A., Dong, C.Y., Yang, E.X., Zhou, H.Y., Xie, H,Q., Ma, M.Z., 2012a. Redefinition of depositional ages of Neoarchean supracrustal rocks in western Shandong Province, China: SHRIMP U–Pb zircon dating. Gondwana Research 21, 768–784.

Wan, Y., Dong, C., Liu, D., Kröner, A., Yang, C., Wang, W., Du, L., Xie, H., Ma, M., 2012b. Zircon ages and geochemistry of late Neoarchean syenogranites in the North China Craton: A review. Precambrian Research 222, 265–289.

Wan, Y.S., Xie, S.W., Yang, C.H., Kröner, A., Ma, M.Z., Dong, C.Y., Du, L.L., Xie, H.Q., Liu, D.Y., 2014a. Early Neoarchean (~2.7 Ga) tectono-thermal events in the North China Craton: A synthesis. Precambrian Research 247, 45–63.

Wan, Y.S., Dong, C.Y., Wang, S.J., Kröner, A., Xie, H.Q., Ma, M.Z., Zhou, H.Y., Xie, S.W., Liu, D.Y., 2014b. Middle Neoarchean magmatism in western Shandong, North China Craton: SHRIMP zircon dating and LA-ICP-MS Hf isotope analysis. Precambrian Research 255, 865–884.

Wan, Y.S., Liu, D.Y., Dong, C.Y., Xie, H.Q., Kröner, A., Ma, M.Z., Liu, S.J., Xie, S.W., Ren, P., 2015. Formation and evolution of Archean continental crust of the North China Craton, in: Zhai MG (Ed.) Precambrian geology of China. Springer, pp. 59–136.

Wang, S.J., Li, S.G., Chen, L.J., He, Y.S., An, S.C., Shen, J., 2013. Geochronology and geochemistry of leucosomes in the North Dabie Terrane, East China: implication for post-UHPM crustal melting during exhumation. Contributions to Mineralogy and Petrology 165, 1009–1029.

Ward, R., Stevens, G., Kisters, A., 2008. Fluid and deformation induced partial melting and melt volumes in low-temperature granulite-facies metasediments, Damara Belt, Namibia. Lithos 105, 253–271.

Watkins, J.M., Clemens, J.D., Treloar, P.J., 2007. Archaean TTGs as sources of younger granitic magmas: melting of sodic metatonalites at 0.6–1.2 GPa. Contributions to Mineralogy and Petrology 154, 91–110.

Weinberg, R.F., Hasalová, P., 2015. Water-fluxed melting of the continental crust: A review. Lithos 212–215, 158–188.

Whalen, J.B., Percival, J.A., McNicoll, V.J., Longstaffe, F.J., 2002. A mainly crustal origin for tonalitic granitoid rocks, Superior Province, Canada: Implications for Late Archean tectonomagmatic processes. Journal of Petrology 43, 1551–1570.

White, R.W., Powell, R., 2010. Retrograde melt–residue interaction and the formation of near-anhydrous leucosomes in migmatites. Journal of Metamorphic Geology 28, 579–597.

Winther, K.T., 1996. An experimentally based model for the origin of tonalitic and trondhjemitic melts. Chemical Geology 127, 43–59.

Wolfram, L.C., Weinberg, R.F., Hasalová, P., Becchio, R., 2017. How Melt Segregation Affects Granite Chemistry: Migmatites from the Sierra de Quilmes, NW Argentina. Journal of Petrology 58, 2339–2364.

Table captions
Table 1. Sample list, rock types and sampling locations.

Figure Captions
Fig. 1. Simplified geological map of the Western Shandong Province. Modified from Cao (1996) and Wan et al. (2011). The star is the location of the samples in this study. The inset shows the extent of the North China Craton (NCC) and the Western Shandong Province (WSP).

Fig. 2. Representative field photographs of leucosomes in the metatonalite. (a) Discordant patch leucosome with relatively coarse-grained hornblende compared with the melanosome. (b) Close-up view of the leucosome in (a). (c) Stromatic leucosome that is in petrographic continuity with discordant leucosome. Both contain coarse-grained hornblende. (d) Discordant leucosome in petrographic continuity with stromatic leucosome. None of the leucosomes contain mafic selvedges at their margins.

Fig. 3. Representative microstructures of metatonalite (a, b) and amphibolite (c, d). (a) Rounded biotite inclusions in coarse-grained hornblende in the leucosome of a metatonalite. (b) Melanosome of metatonalite. (c) Coarse interlocking plagioclase with interstitial quartz in a leucosome. (d) Veinlet with abundant coarse-grained hornblende. (e) Coarse-grained hornblende with rounded inclusions of biotite in the leucosome of an amphibolite. (f) Melanosome of an amphibolite. All photographs are in plane-polarized light.

Fig. 4. Representative field photographs of leucosomes in the amphibolite. (a) Meter-scale enclave of amphibolite in metatonalite. (b) Strongly deformed gneiss of metatonalite and amphibolite. (c) Patch leucosome with coarse-grained hornblende relative to the melanosome. (d) Close-up view of the leucosome in (c). (e) Patch leucosome in a mafic enclave in a host metatonalite. (f) Discontinuous hornblende-bearing 'patch' leucosomes in amphibolite.

Fig. 5. Hornblende and plagioclase compositions. (a) Hornblende compositions plotted on the classification diagram of Leake et al. (1997). (b) Alkali elements versus silicon for hornblende. (c) Titanium versus silicon for hornblende. (d) Plagioclase compositions, X_{An} = molar (Ca / [Ca + Na + K]). Atoms per formula unit (a.p.f.u.). On the box-and-whisker plots, the whiskers extend to the lowest and highest datum inside 1.5 times the interquartile range and outliers (represented by crosses) are outside of this range. (e) Chondrite-normalized rare earth element concentrations of hornblende from metatonalite. (f) Chondrite-normalized rare earth element concentrations of hornblende from amphibolite.

Fig. 6. Major element oxide data for metatonalite and amphibolite samples from this study as well as ~2.5 Ga granites from Peng et al. (2013) and Wan et al. (2012b).

Fig. 7. Trace element data for paired leucosome–melanosome samples (connected by lines).

Fig. 8. Chondrite-normalized rare earth element (REE) profiles for the melanosome and leucosome samples from the metatonalite and the amphibolite. Normalization values are from McDonough and Sun (1995).

Fig. 9 Chondrite-normalized rare earth element (REE) patterns for paired melanosome–leucosome samples from the metatonalite and the amphibolite. Except for samples T026, T029B and T029C (stromatic leucosomes), the other paired samples show similar trends.

Fig. 10. Box-and-whisker plots of the enrichment factor (quotient of the leucosomes concentrations divided by the melanosome concentrations) in leucosomes for paired samples interpreted to represent near primary melt compositions of the metatonalite (a) and the amphibolite (b). The box and whisker plots show the distribution of enrichment factors for six samples of the metatonalite and three samples of the amphibolite. Samples T026 and T029B are not included as discussed in the text. SiO_2, Na_2O and Sr are the only elements with median enrichment factors greater than 1. On the box-and-whisker plots, the whiskers extend to the lowest and highest datum inside 1.5 times the interquartile range and outliers (represented by crosses) are outside of this range.

Fig. 11. Oxygen isotope compositions (relative to VSMOW) for paired samples. Except for amphibolite samples T025AL, T025AM and T027A, the values for all samples plot within or above those expected for juvenile material derived from the mantle. The values of T025A suggest oxygen isotope exchange with a low-^{18}O fluid (meteoric water or seawater).

Fig. 12. Mass balance model adding 1–20 wt.% hornblende to the composition of leucosome from sample T026L. Average hornblende is the average REE concentration of hornblende (not including the single LREE-depleted analysis; Fig 5e) from leucosomes in metatonalites (n=5). The HREE concentrations of the leucosome samples T029BL and T026L with >5 wt.% hornblende added are broadly consistent with the concentration of the HREE in the other metatonalite leucosome samples.

Fig. 13. (a) Molar Na+Ca, Fe+Mg+Ti, K ternary diagram (after Solar and Brown, 2001) illustrating the composition of leucosomes interpreted to represent near primary melt compositions and paired

melanosomes relative to the results of experimental fluid-present partial melting studies of similar rock types. Leucosome compositions plot towards the Na+Ca apex away from the Fe+Mg+Ti and K apices. (b) Normative An–Ab–Or (after Barker, 1979) with CIPW normalized modes of paired leucosome–melanosome samples as well as experimental results of partial melting in similar rock types. The leucosomes plot towards the Ab–An join away from the Or apex, which is opposite to the trends observed in fluid-present partial melting studies of tonalite (Watkins et al., 2007). Fluid-present partial melting of metatonalite from the Western Shandong Province produces relatively more plagioclase-rich melt. Experimental data for water-saturated melting for rocks of similar compositions to those of the metatonalite and amphibolite, including: experiments SC4 and SC5 of Watkins et al. (2007) at ~6 kbar and 680–730°C; experimental runs 557, 555, 578, 466 and 571 from Beard and Lofgren (1991) at 6.9 kbar and 800C; two experiments from Winther (1996) include 407B (9kbar, 838°C) and 508B (6 kbar, 795°C).

Fig. 14. Normative An–Ab–Or (after Barker, 1979) showing a comparison of melt compositions from phase equilibria modelling of MORB partial melting (Palin et al., 2016) and leucosome compositions reflecting fluid-present partial melting from this study and Lee and Cho (2013) from the western Gyeonggi Massif, Korea. Trondhjemite and Na-rich tonalite components of Archean TTG suites can reflect both high-temperature melting of mafic rocks or relatively low temperature fluid-present melting of tonalite, diorite and amphibolite.
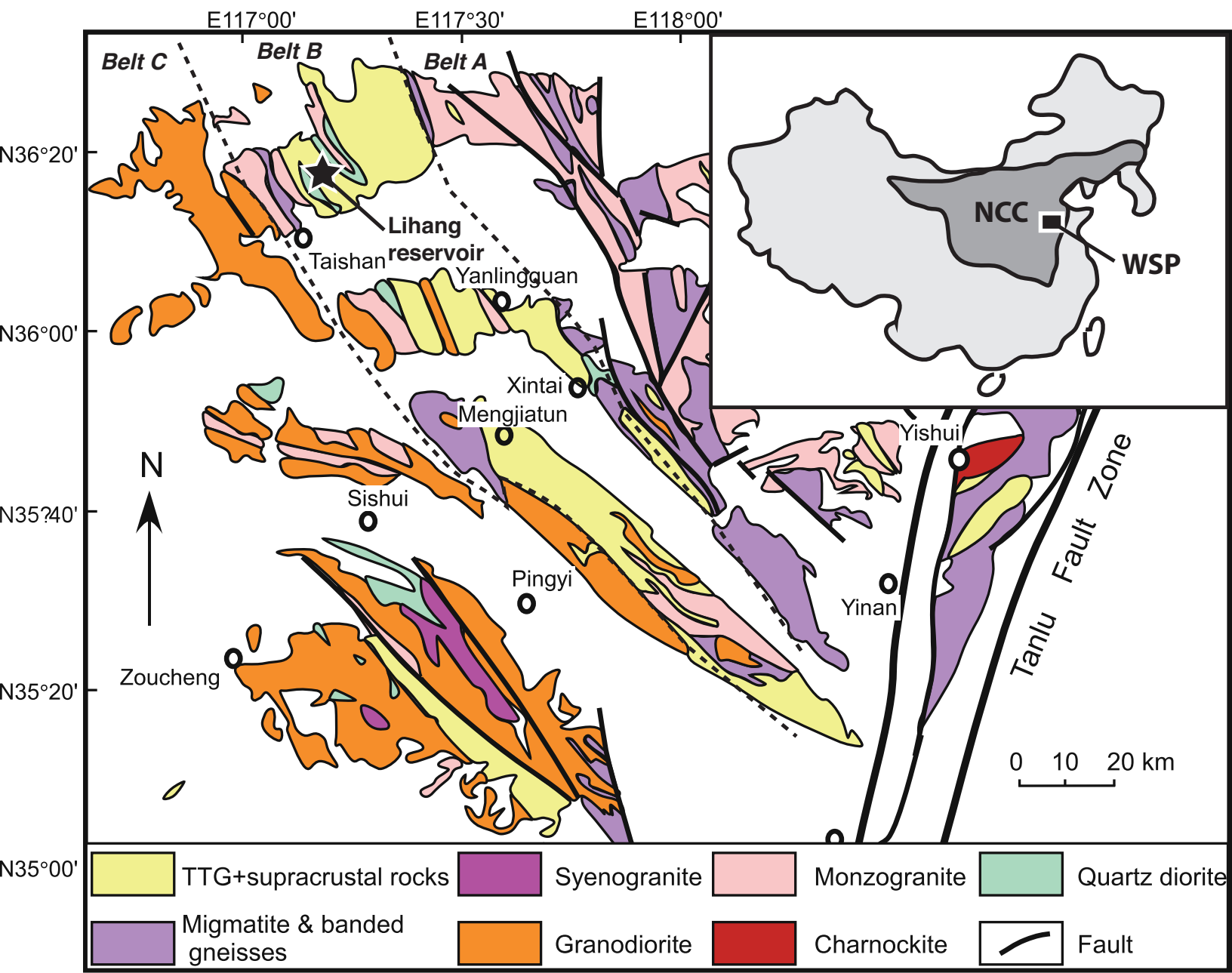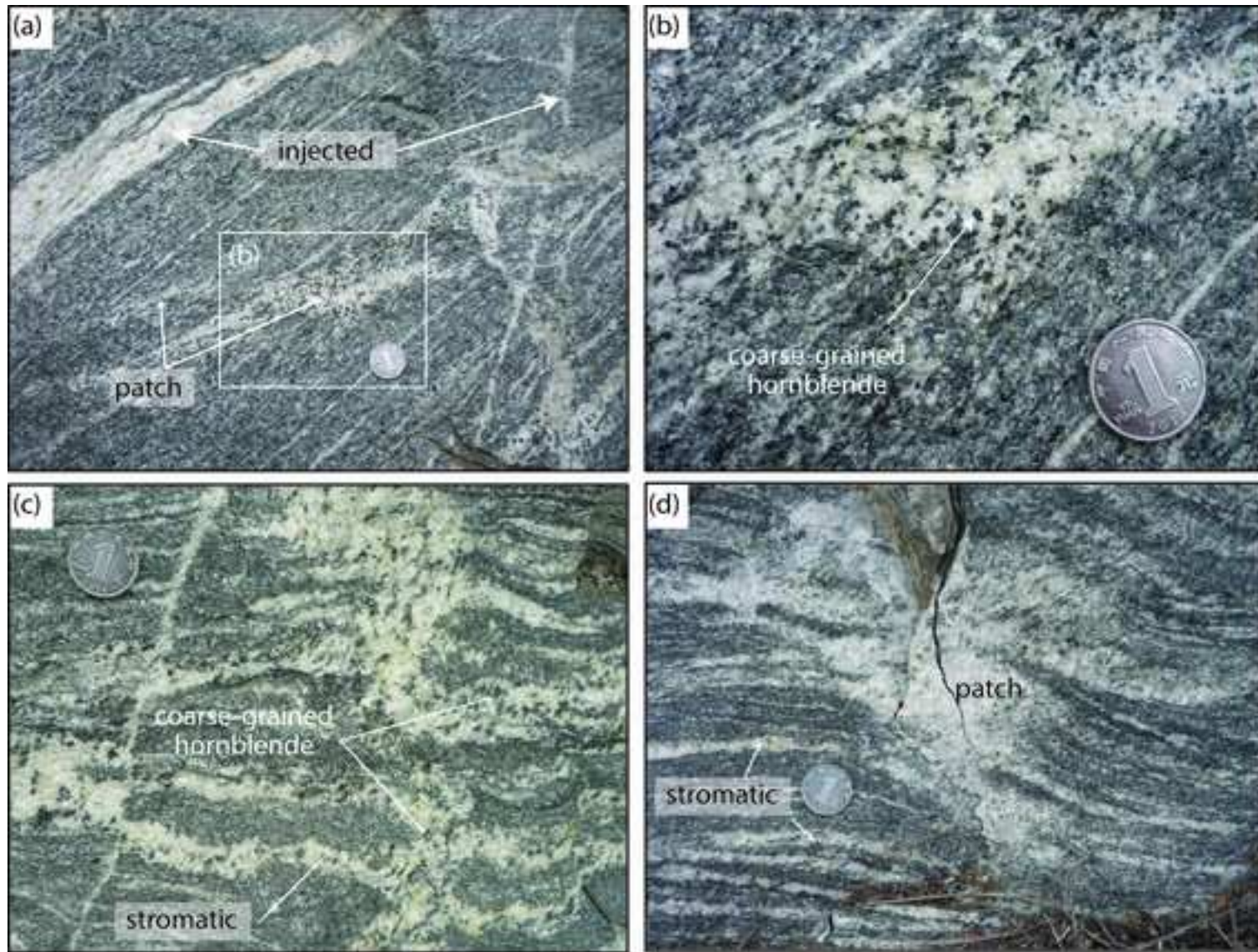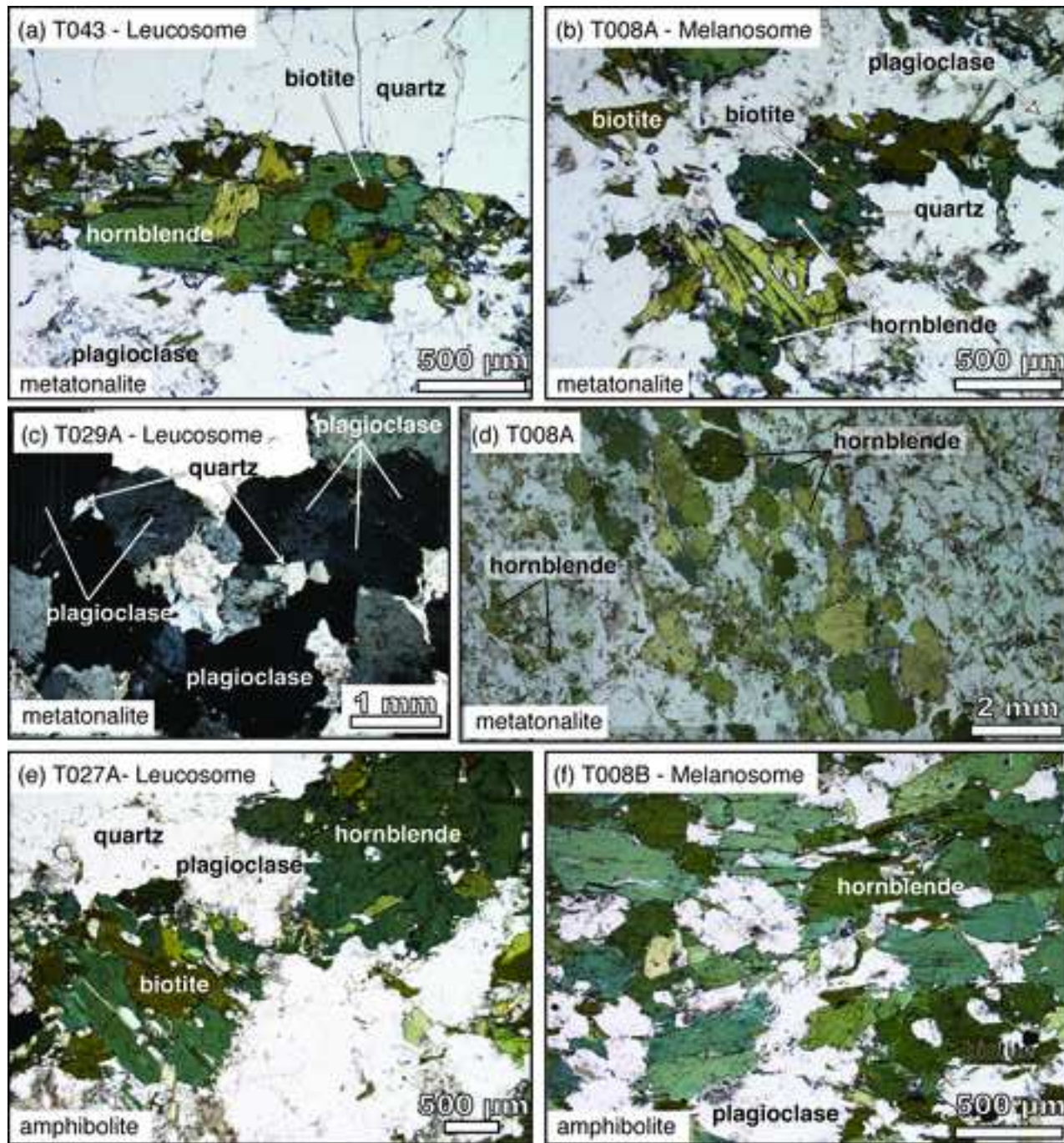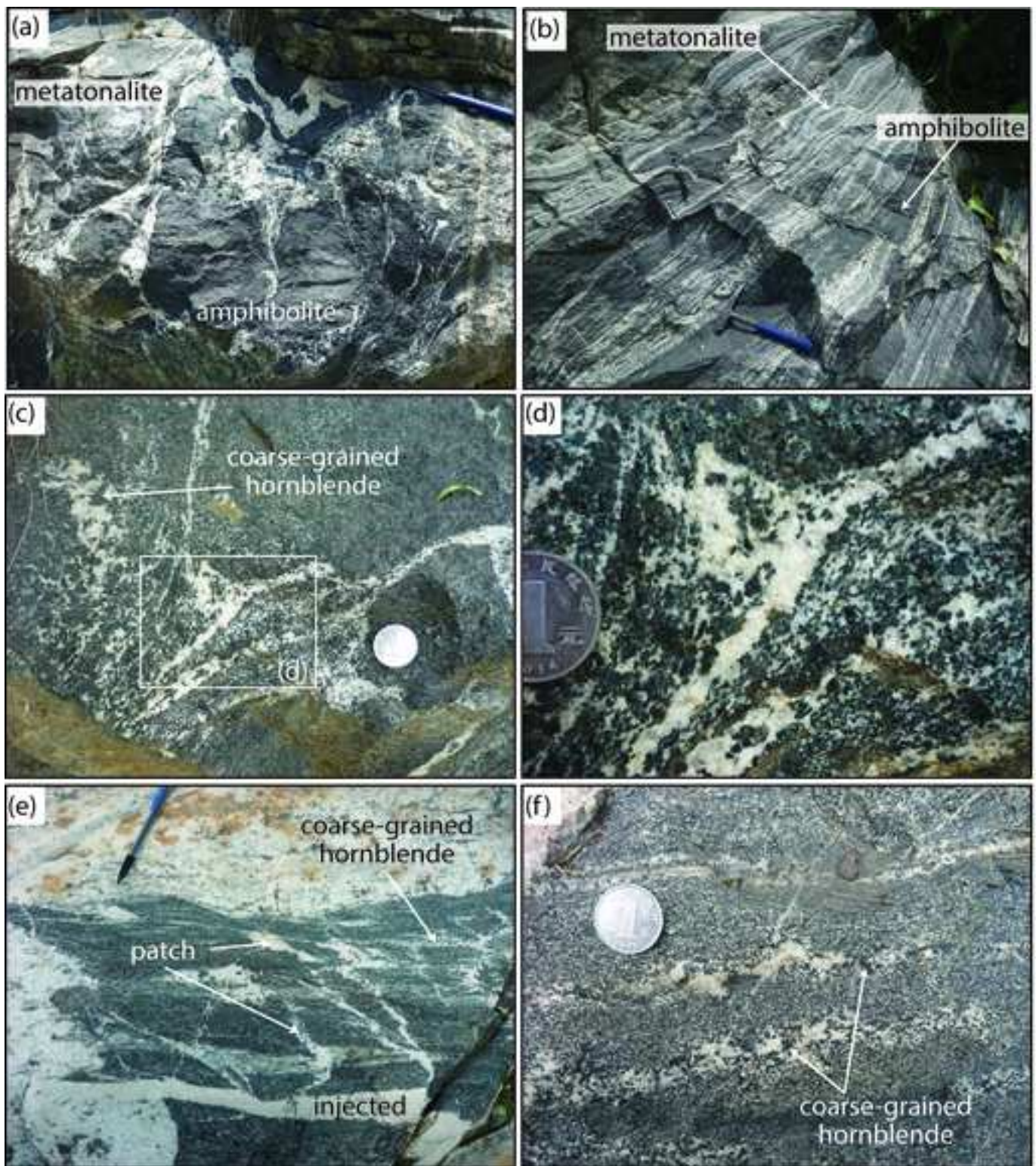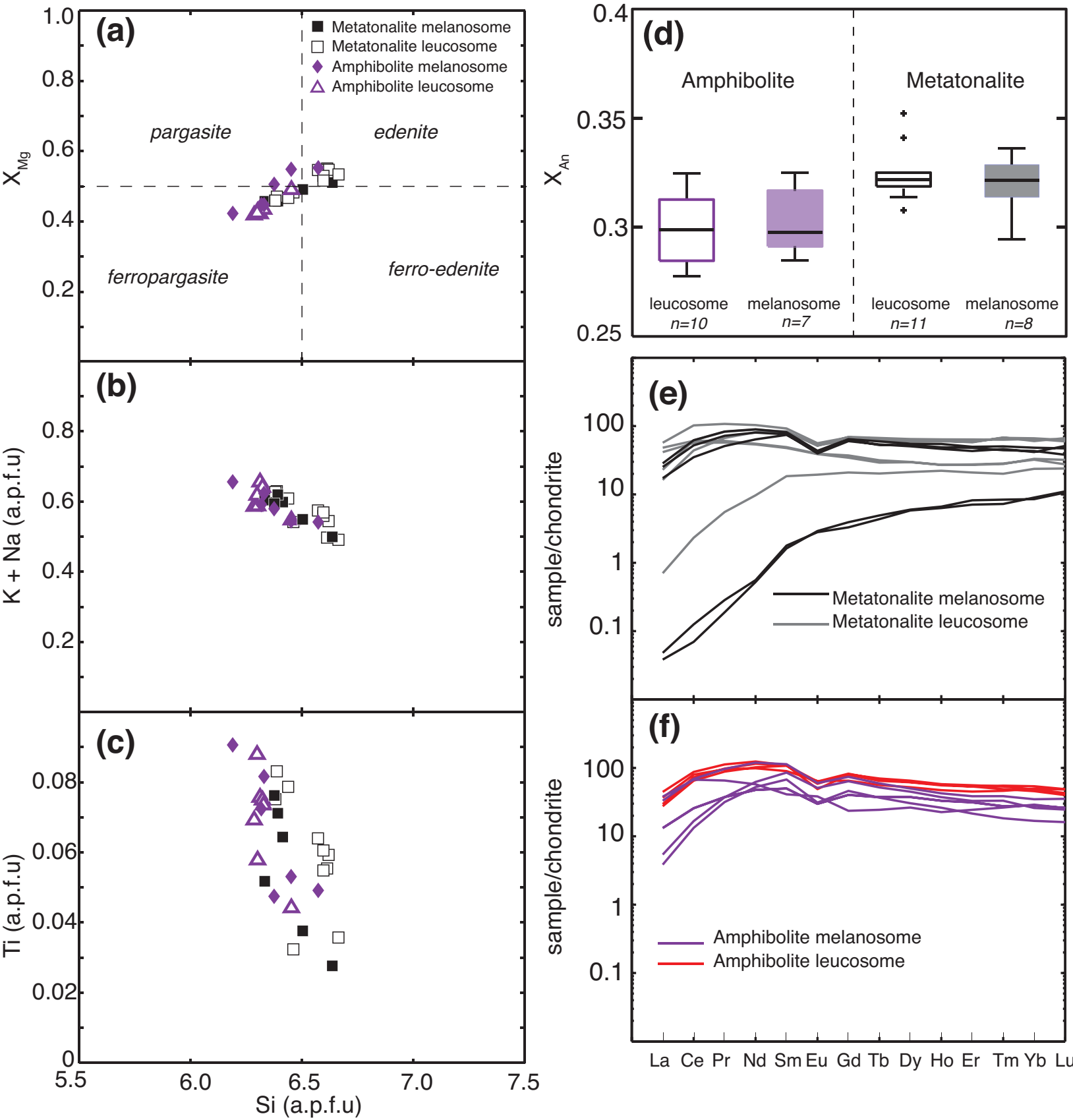
Figure 1

Figure 2

Figure 3

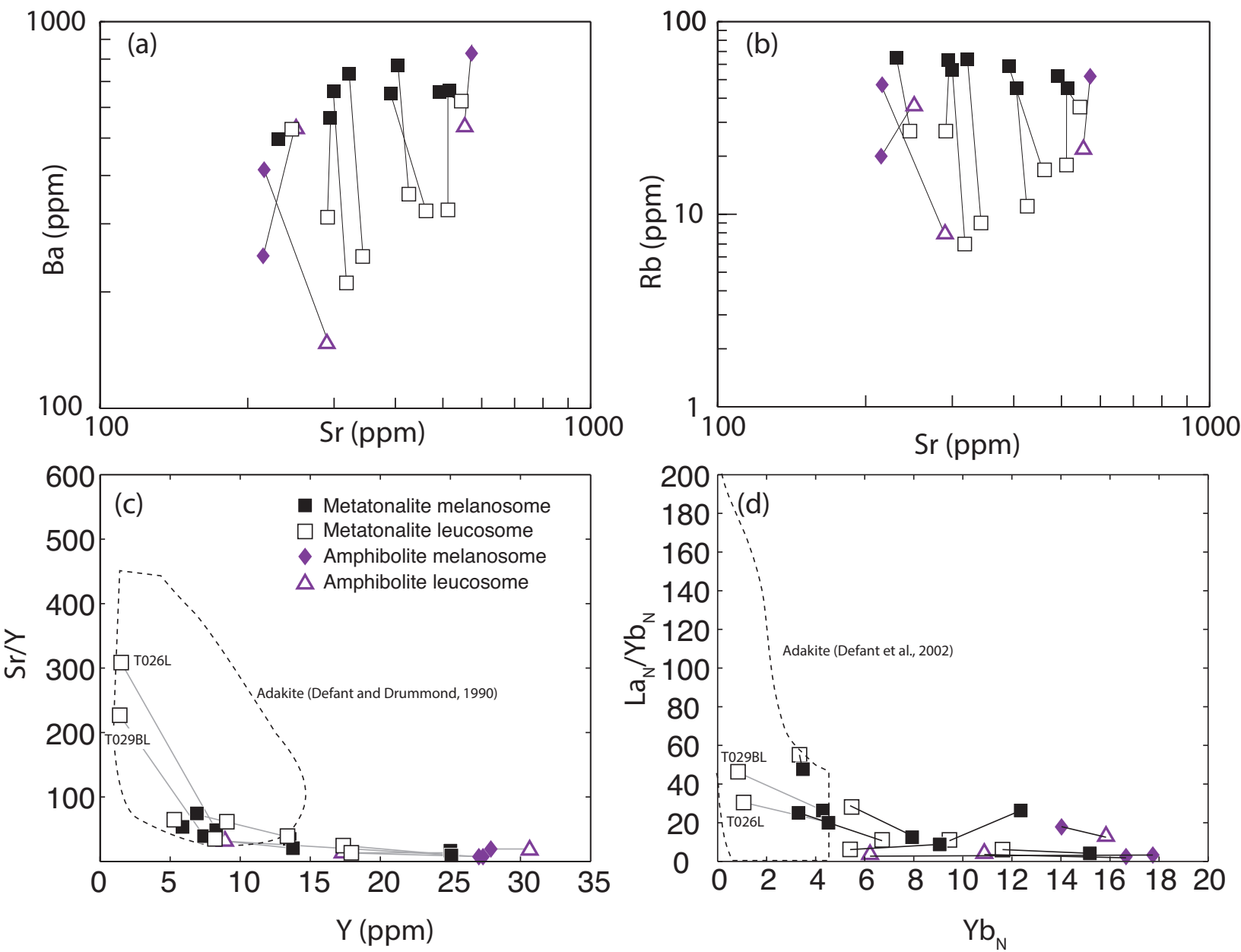**Figure 4**
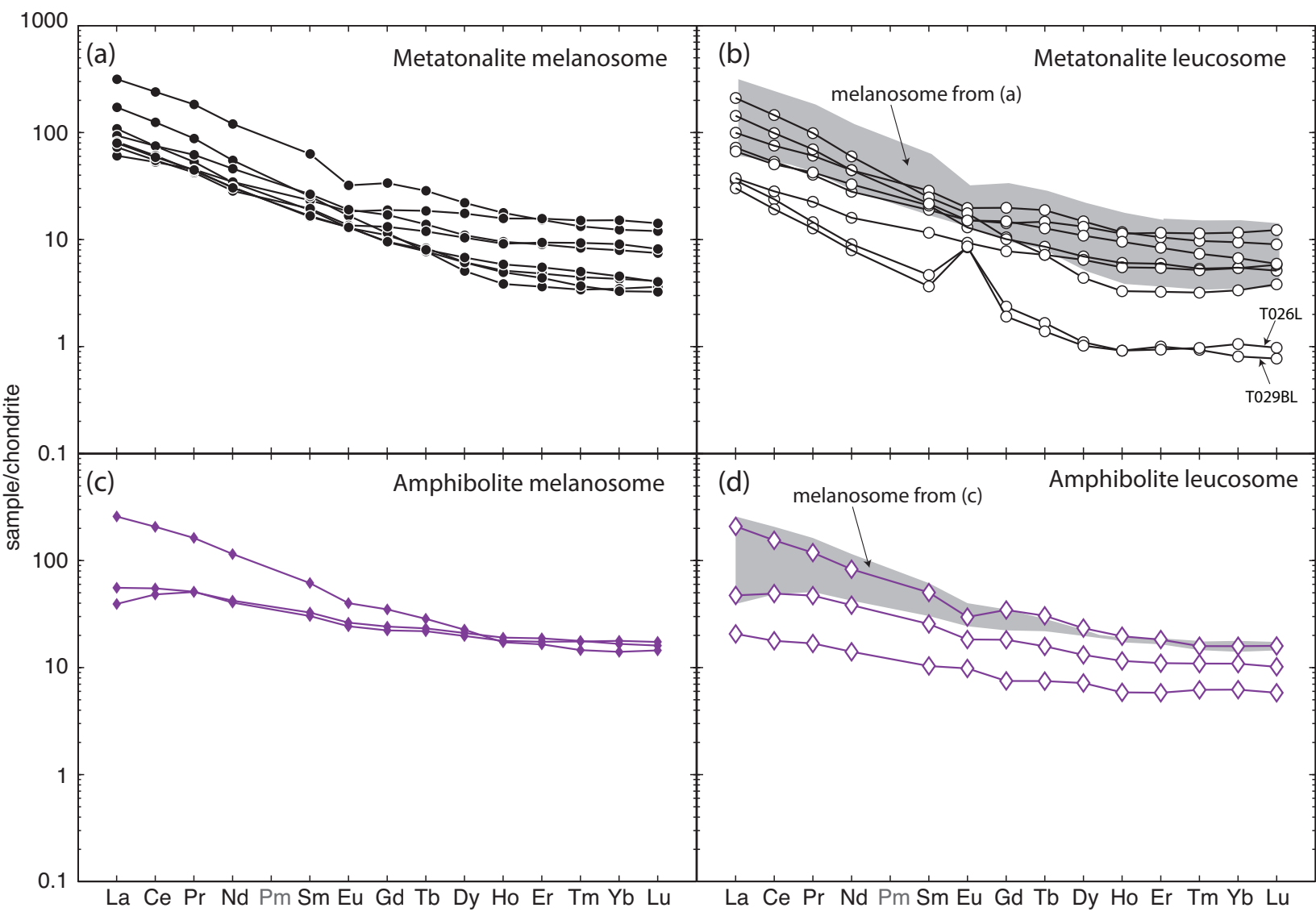
Figure 5

Figure 5

Figure 6
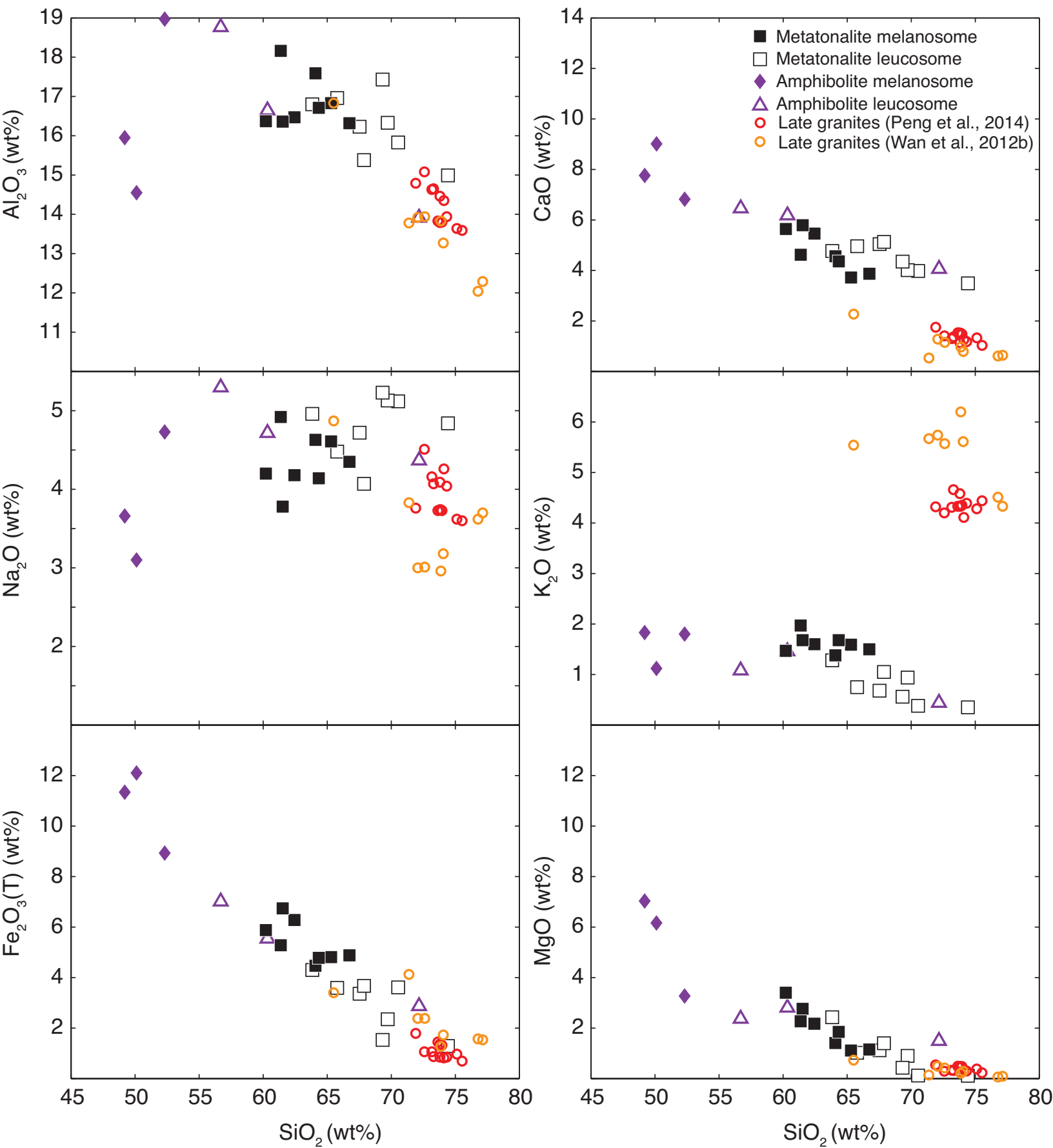
Figure 6

Figure 7

Figure 7

Figure 8

Figure 8

Figure 9

Metatonalite

Amphibolite

(a) T043 Patch — melanosome, leucosome

(b) T008C Patch

(i) T027A

(c) T028C Stromatic

(d) T029A Patch

(j) T025A

(e) T025B Stromatic

(f) T026 Stromatic

(k) T008B

(g) T008A Stromatic

(h) T029B Stromatic

La Ce Pr Nd Pm Sm Eu Gd Tb Dy Ho Er Tm Yb Lu
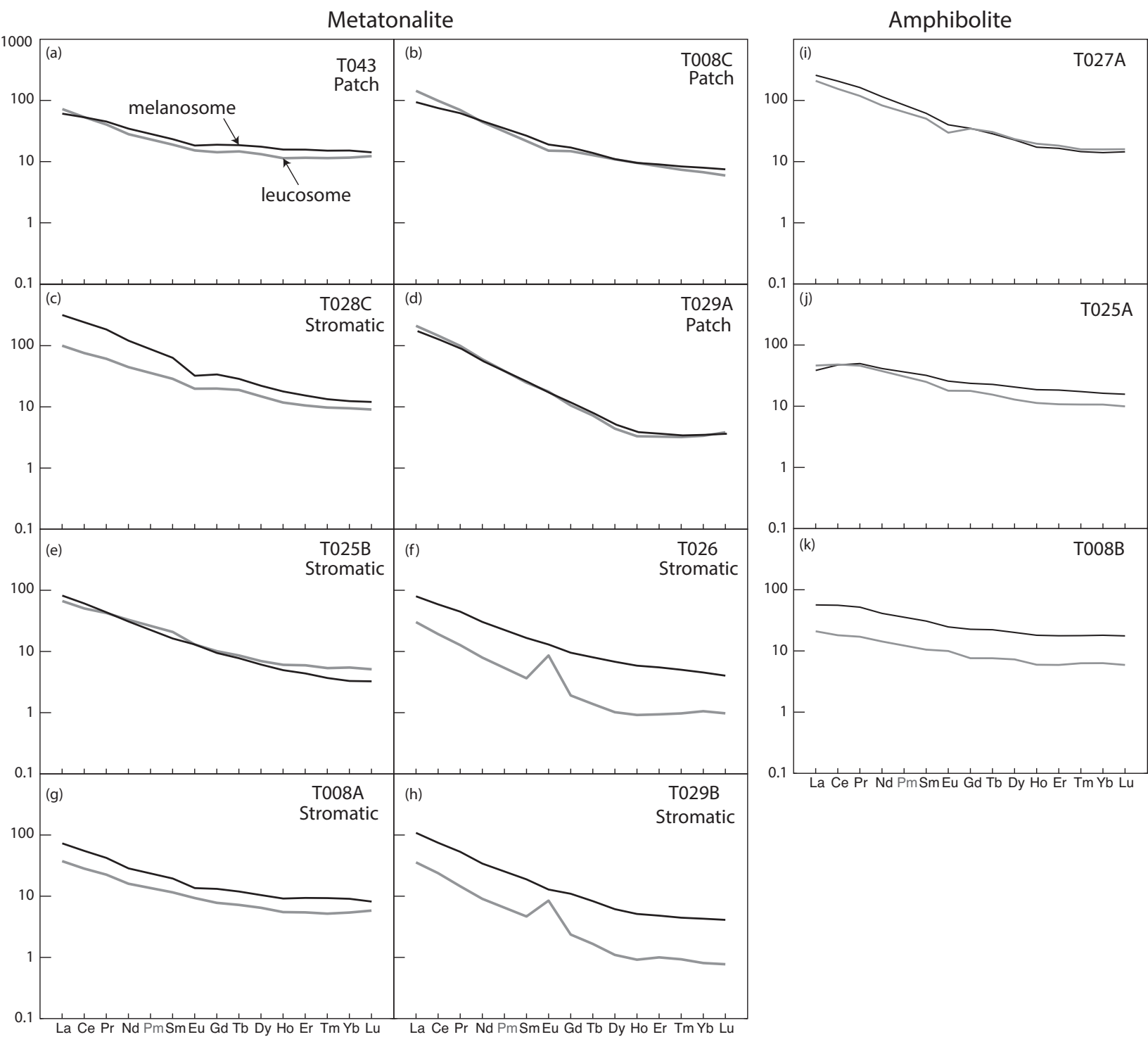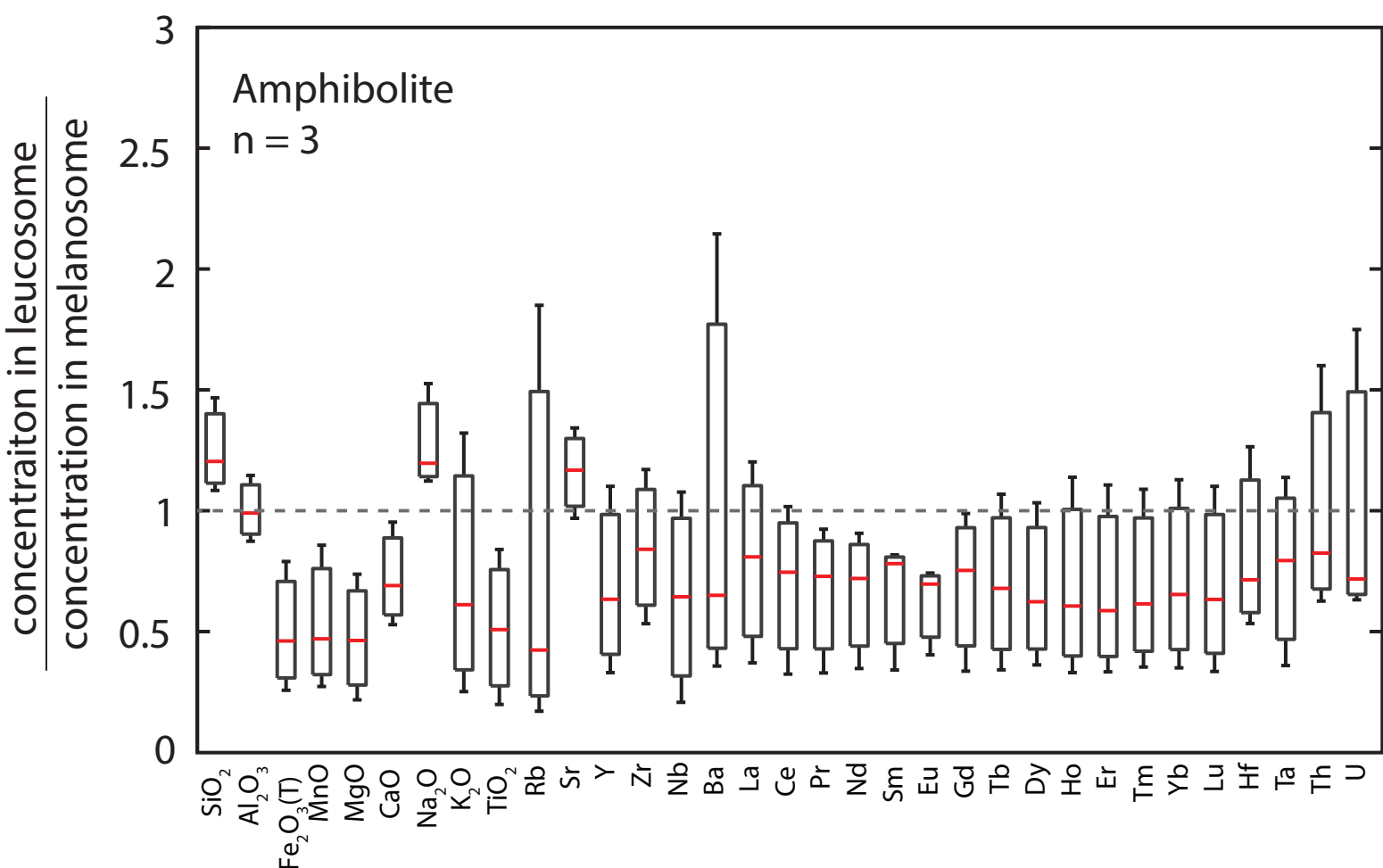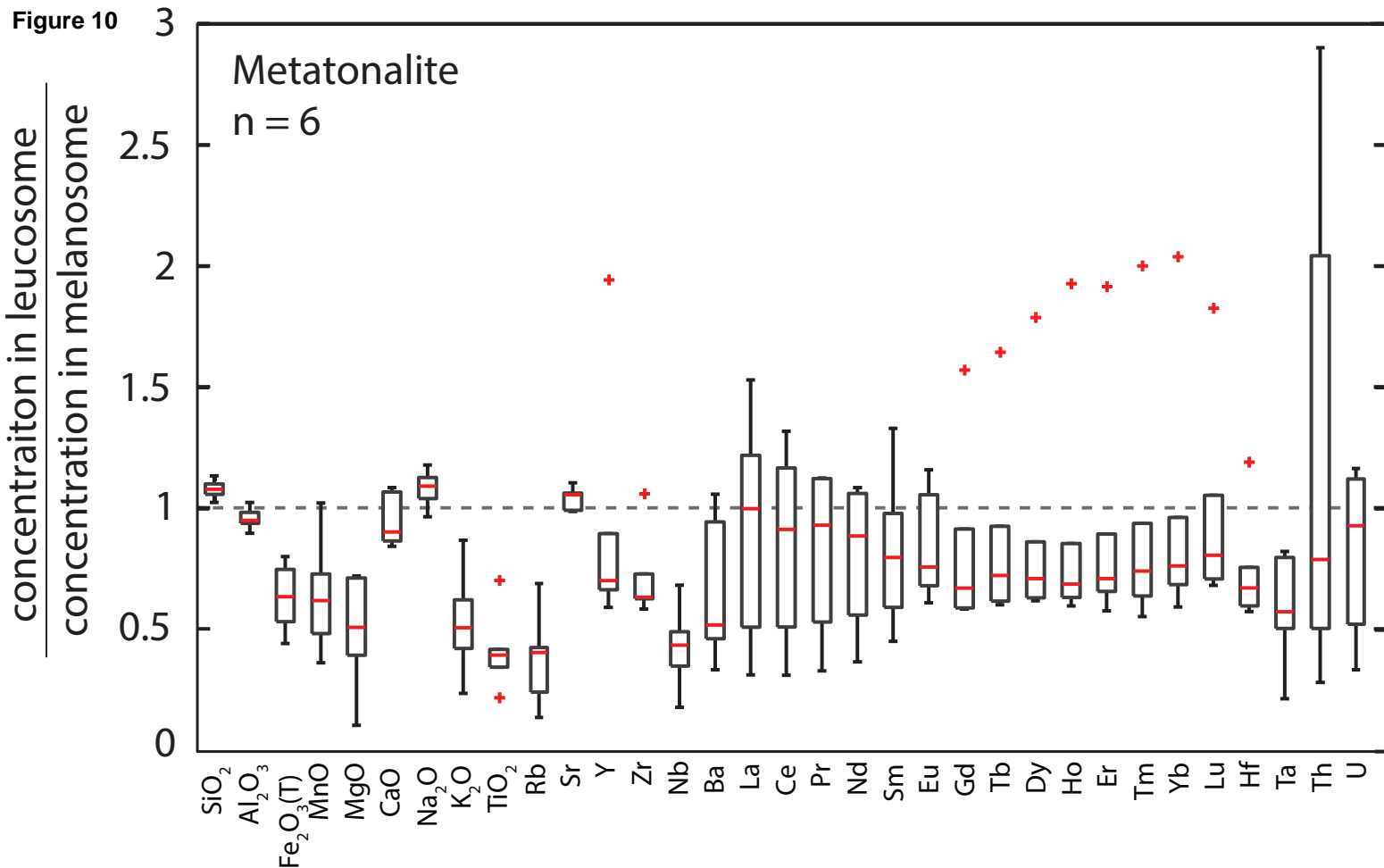
Figure 9

Figure 10

Figure 10

Figure 11
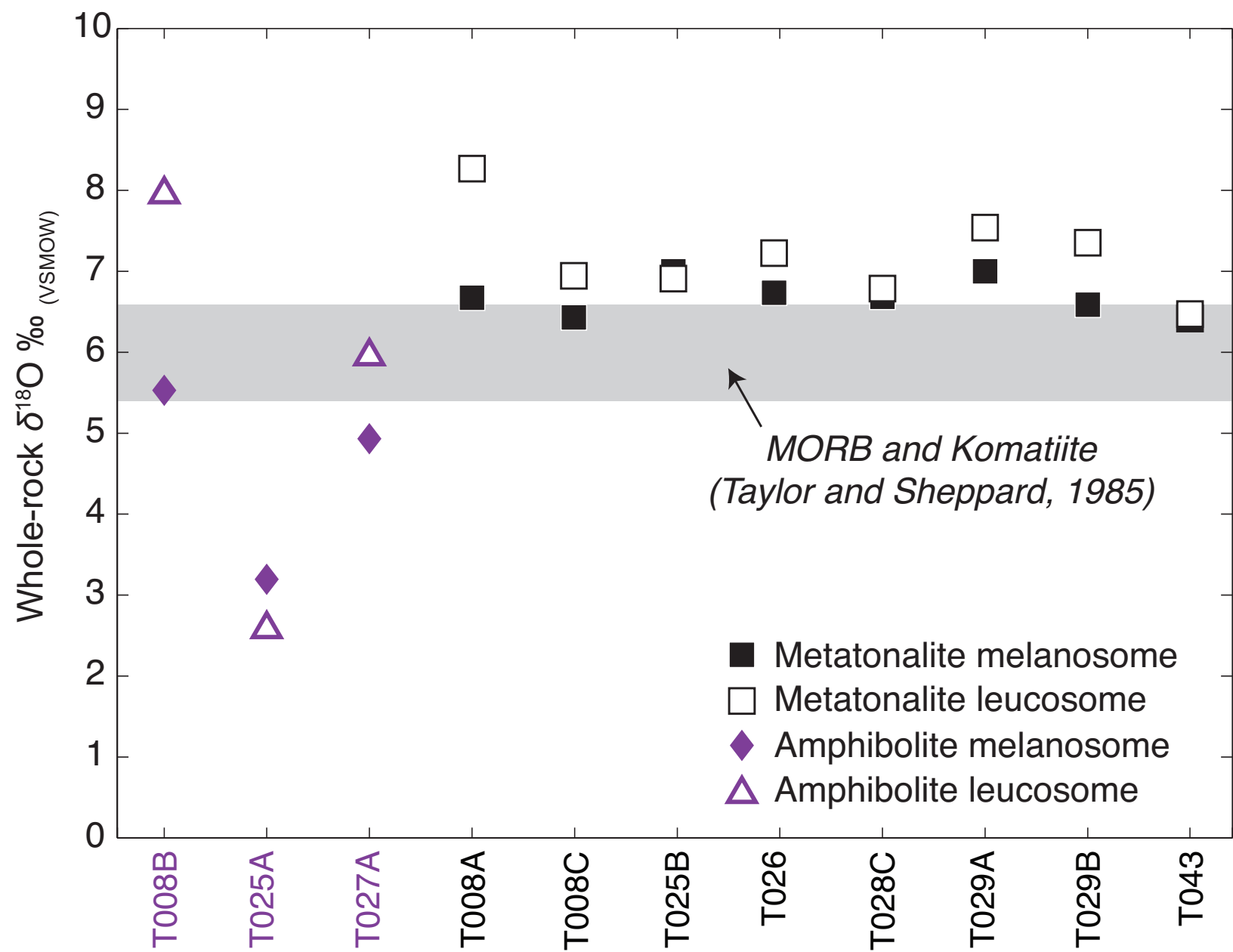
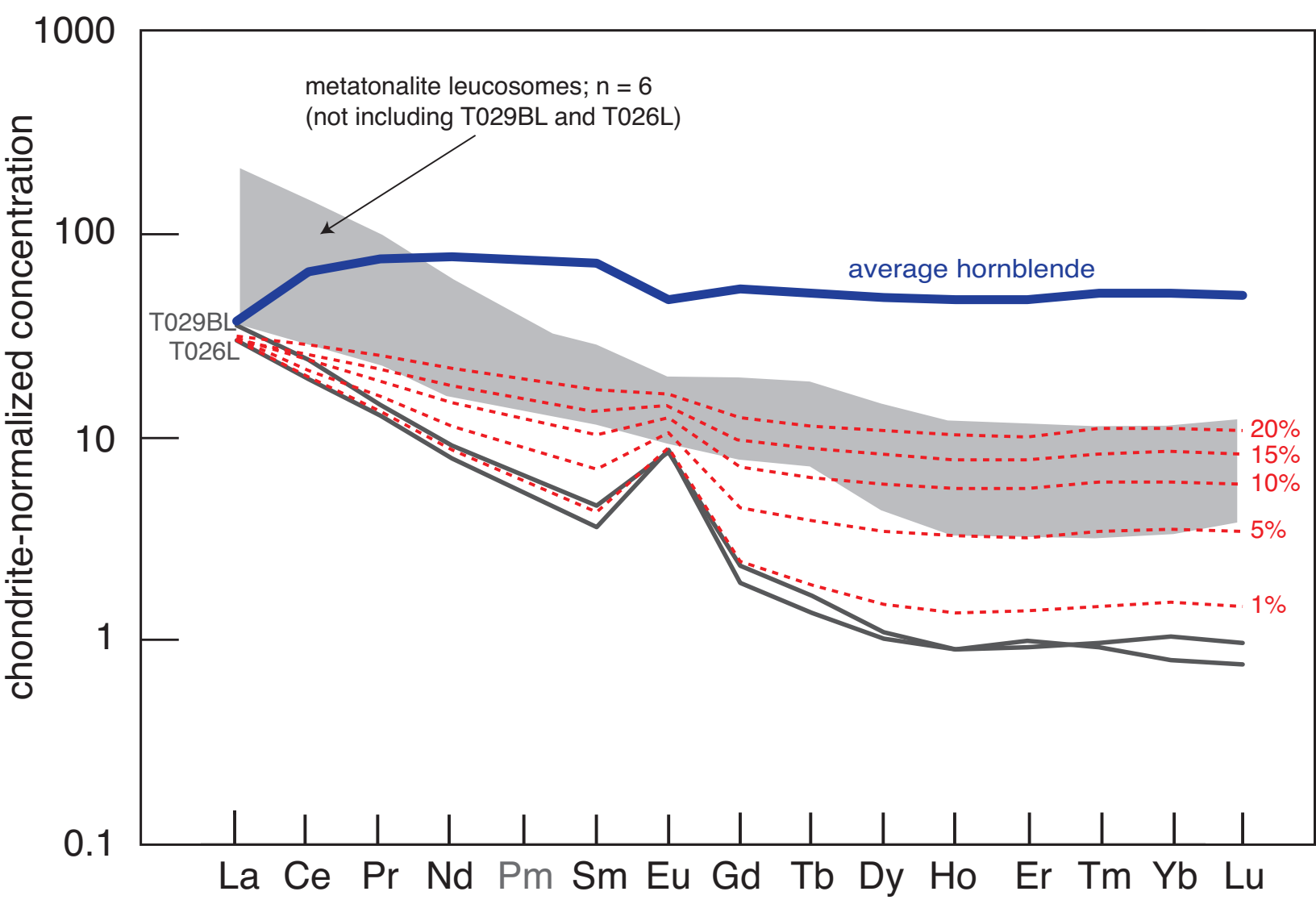**Figure 11**

Figure 12

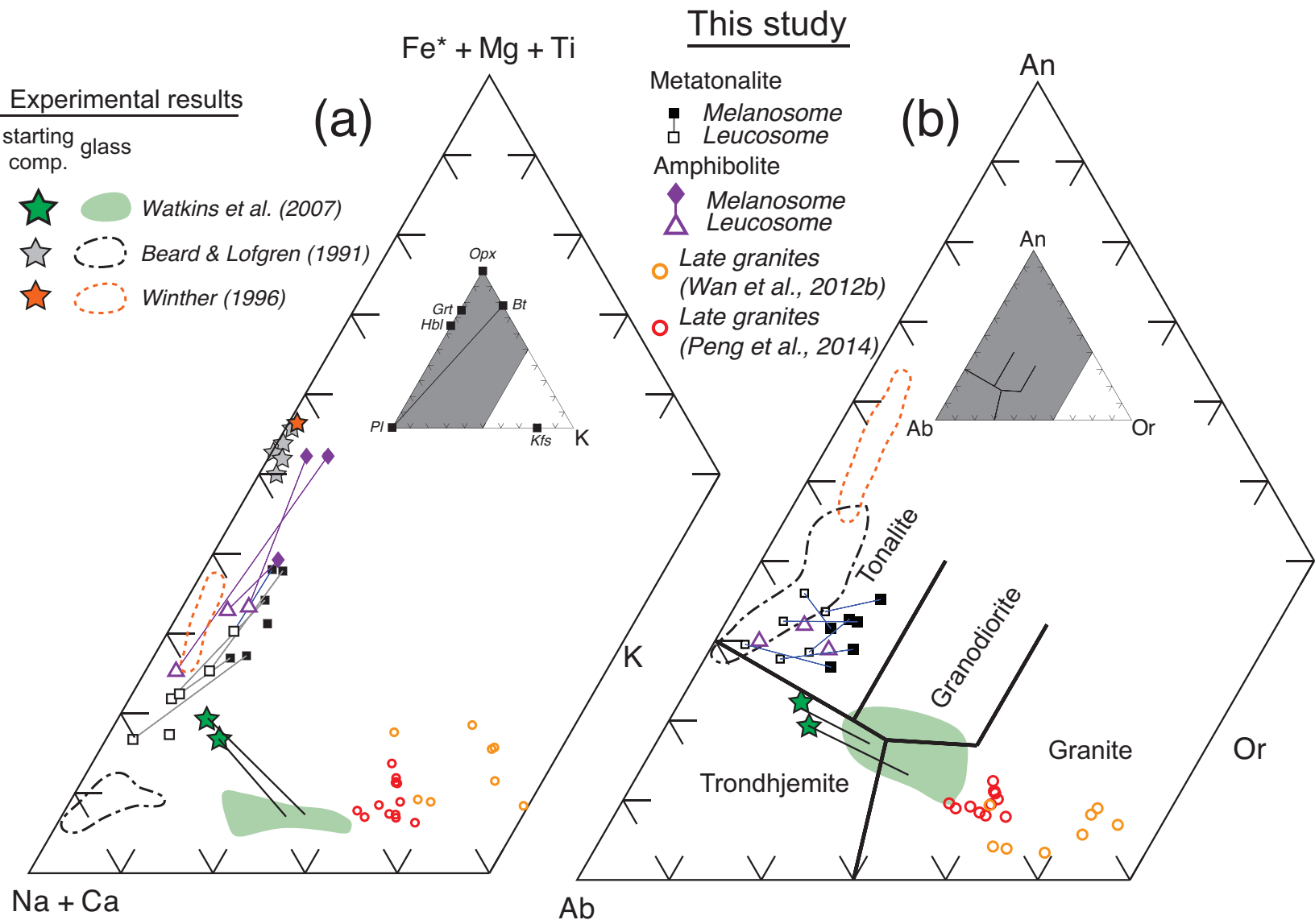**Figure 12**

Figure 13

Figure 13

Figure 14

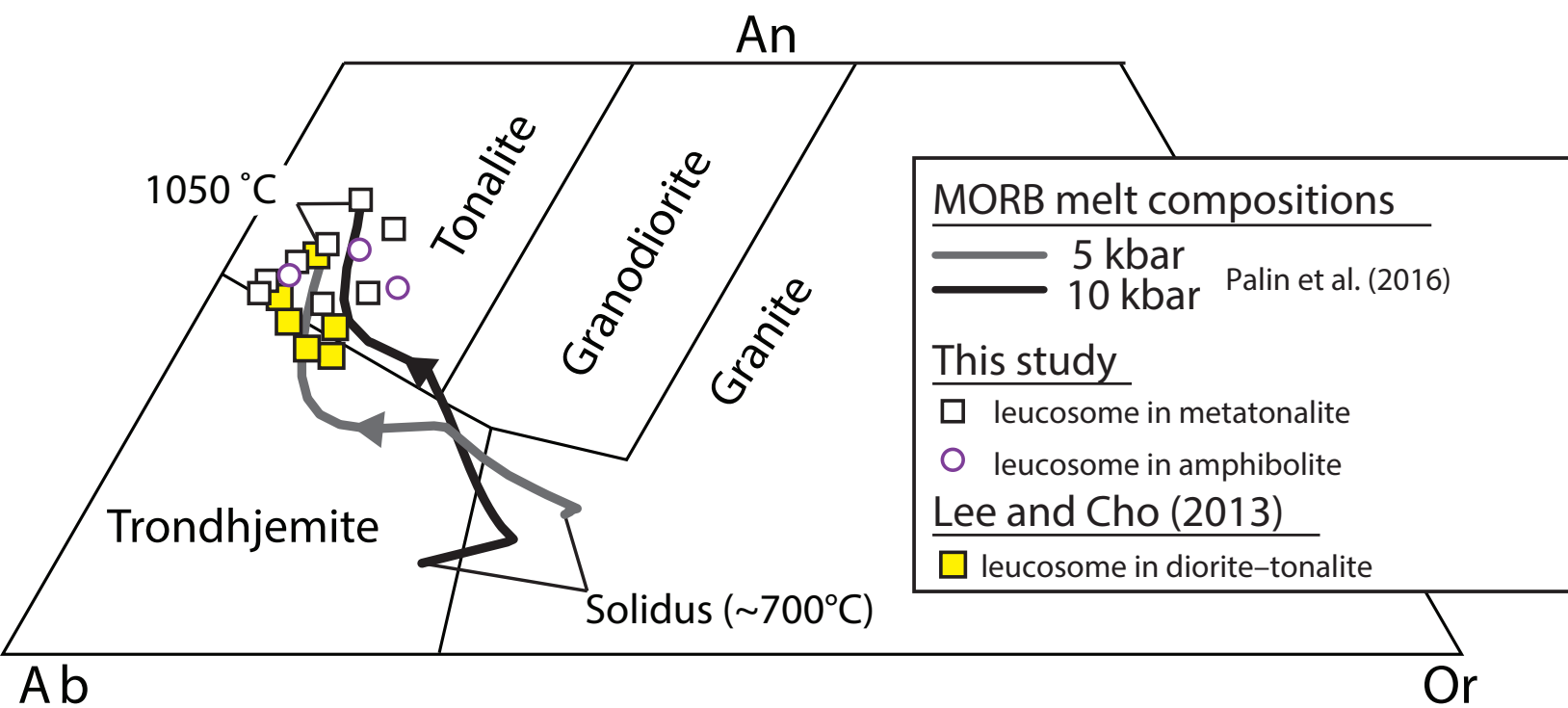**Figure 14**

Table 1.

Sample list and locations (WGS84 datum)

Sample	Rock type	Leuco/Melano	Leucosome Type	Latitude	Longitude
T008BL	Amphibolite	Leucosome	Patch	36°17.831'N	117°09.337'E
T025AL	Amphibolite	Leucosome	Patch	36°17.948'N	117°09.418'E
T027AL	Amphibolite	Leucosome	Patch	36°18.369'N	117°09.774'E
T008BM	Amphibolite	Melanosome	–	36°17.831'N	117°09.337'E
T025AM	Amphibolite	Melanosome	–	36°17.948'N	117°09.418'E
T027AM	Amphibolite	Melanosome	–	36°18.369'N	117°09.774'E
T029AL	Tonalite Gneiss	Leucosome	Patch	36°18.517'N	117°09.871'E
T008CL	Tonalite Gneiss	Leucosome	Patch	36°17.831'N	117°09.337'E
T043L	Tonalite Gneiss	Leucosome	Patch	36°18.378'N	117°09.504'E
T029AM	Tonalite Gneiss	Melanosome	–	36°18.517'N	117°09.871'E
T008CM	Tonalite Gneiss	Melanosome	–	36°17.831'N	117°09.337'E
T043M	Tonalite Gneiss	Melanosome	–	36°18.378'N	117°09.504'E
T008AL	Tonalite Gneiss	Leucosome	Stromatic	36°17.831'N	117°09.337'E
T025BL	Tonalite Gneiss	Leucosome	Stromatic	36°17.948'N	117°09.418'E
T026L	Tonalite Gneiss	Leucosome	Stromatic	36°18.201'N	117°10.107'E
T028CL	Tonalite Gneiss	Leucosome	Stromatic	36°18.480'N	117°09.863'E
T029BL	Tonalite Gneiss	Leucosome	Stromatic	36°18.517'N	117°09.871'E
T008AM	Tonalite Gneiss	Melanosome	–	36°17.831'N	117°09.337'E
T025BM	Tonalite Gneiss	Melanosome	–	36°17.948'N	117°09.418'E
T026M	Tonalite Gneiss	Melanosome	–	36°18.201'N	117°10.107'E
T028CM	Tonalite Gneiss	Melanosome	–	36°18.480'N	117°09.863'E
T029BM	Tonalite Gneiss	Melanosome	–	36°18.517'N	117°09.871'E